Materials Today Bio 23 (2023) 100894

Contents lists available at ScienceDirect

Materials Today Bio

journal homepage: www.journals.elsevier.com/materials-today-bio

Melanin/melanin-like nanoparticles: As a naturally active platform for imaging-guided disease therapy

Jinghua Sun [a], Yahong Han [c], Jie Dong [c], Shuxin Lv [c], Ruiping Zhang [a,b,*]

[a] The Molecular Medicine Research Team of First Hospital of Shanxi Medical University, Taiyuan, 030001, China
[b] The Radiology Department of Shanxi Provincial People' Hospital, Five Hospital of Shanxi Medical University, Taiyuan, 030001, China
[c] Shanxi Medical University, Taiyuan 030001, China

ARTICLE INFO

Keywords:
melanin nanoparticles
Melanin-like nanoparticles
Imaging-guided
Therapeutic platform

ABSTRACT

The development of biocompatible and efficient nanoplatforms that combine diagnostic and therapeutic functions is of great importance for precise disease treatment. Melanin, an endogenous biopolymer present in living organisms, has attracted increasing attention as a versatile bioinspired functional platform owing to its unique physicochemical properties (e.g., high biocompatibility, strong chelation of metal ions, broadband light absorption, high drug binding properties) and inherent antioxidant, photoprotective, anti-inflammatory, and antitumor effects. In this review, the fundamental physicochemical properties and preparation methods of natural melanin and melanin-like nanoparticles were outlined. A systematical description of the recent progress of melanin and melanin-like nanoparticles in single, dual-, and tri-multimodal imaging-guided the visual administration and treatment of osteoarthritis, acute liver injury, acute kidney injury, acute lung injury, brain injury, periodontitis, iron overload, etc. Was then given. Finally, it concluded with a reasoned discussion of current challenges toward clinical translation and future striving directions. Therefore, this comprehensive review provides insight into the current status of melanin and melanin-like nanoparticles research and is expected to optimize the design of novel melanin-based therapeutic platforms and further clinical translation.

1. Introduction

Imaging-guided disease therapy, combining diagnostic and therapeutic modalities within a single platform, not only could monitor the real-time distribution and the release behaviour of the therapeutic agents in tissues but could reveal the optimized treatment time and dose within lesion sites under the guidance of diverse bio-imaging methods, which obtains more excellent therapeutic efficacy and has developed into a new candidate in many disease therapies [1–3]. In the case of cancer treatment, an ideal theranostic agent not only provides a accurate assessment of detailed tumor characteristics (e.g., location, size, and shape) through various imaging modalities but also allows targeted delivery of various therapeutic agents, such as antitumor drug, photothermal agents, photosensitizer, immunoadjuvant, and so forth [4,5]. Recently, enormous theranostic nanoplatforms have been explored for imaging-guided disease therapy, including metal-based [6–8], carbon-based [9], calcium-based [10], silica-based [11–13], conjugated polymers, and nano-complexes containing small molecule organic dyes [14], and so on. However, few of them have been translated into clinical studies considering their potential long-term toxicity (see Tables 3 and 4).

Compared with exogenous nanomaterials, natural endogenous biomaterials extracted from organisms have attracted a great deal of attention because of their competence to be decomposed and metabolized in the body so as to cause only negligible side effects, which is essential to ensure their biosafety in vivo. Melanin is a well-known biopolymer widely distributed in almost all living organisms such as animals, plants, microorganisms and even human skin, hair and eyes [15–17]. In recent years, melanin/melanin-like nanoparticles have received increasing attention in the design and construction of multifunctional nanoplatforms for biomedical applications owing to their myriad functions [18–21]. Firstly, melanin/melanin-like nanoparticles possess a large number of metal ion binding sites due to the presence of amine, carboxyl, o-quinone, semi-quinone, phenolic hydroxyl groups and even nitrogen atoms in their structure, making them highly chelating to various metal ions such as Fe^{3+}, Cu^{2+}, Gd^{3+}, Mn^{2+}, etc. [22,23], which is beneficial as a contrast agent for molecular imaging [24]. Secondly, they exhibit a monotonic broadband absorption profile across

* Corresponding author. The Molecular Medicine Research Team of First Hospital of Shanxi Medical University, Taiyuan, 030001, China.
E-mail address: zrp_7142@sxmu.edu.cn (R. Zhang).

https://doi.org/10.1016/j.mtbio.2023.100894
Received 4 October 2023; Received in revised form 23 November 2023; Accepted 29 November 2023
Available online 5 December 2023

the UV–Vis region, giving them the potential for photoacoustic imaging and photothermal therapy [20,25,26]. Additionally, high drug binding performance of melanin/melanin-like nanoparticles coming from π–π stacking, hydrogen bonding interaction, and van der Waals interaction, makes them an ideal choice for drug delivery [27–29]. The large reductive functional groups (e.g., catechol, amine, and imine) also endow these nanoparticles with broad scavenging activities against multiple reactive oxygen and nitrogen free radicals, rendering them perfect antioxidative performance [30–32]. Panzella et al. thought typical structural and p-electron features of melanin (5,6-dihydroxyindole-2-carboxylic acid) lead to superior free-radical-scavenging capabilities [33]. Recent research has found that melanin could help to protect skin cells from UV-induced DNA damage by shielding UV rays and scavenging free radicals [34]. Furthermore, benefitting from large chemically active functional groups (e.g., catechol, o-quinone, amine, and imine), melanin/melanin-like nanoparticles can bond with various nucleophilic thiol- and amino-containing molecules using Michael addition, Schiff base reaction or coordinative interactions [31,35,36]. Besides, these nanoparticles also have other functions such as structural coloration, skin protection, nonradiative relaxation of photoinduced electron states, antibiotic function, and some nervous system involvement [21,37–39].

Together with inherent biocompatibility and biodegradability, fascinating physicochemical properties, mild preparation process, and easy functionalization, melanin/melanin-like nanoparticles have been explored as a promising nanoplatform for diverse biomedical applications. Recently, some excellent reviews have been published with the main emphasis on melanin-based nanomaterials as a versatile platform in biomedicine. For instance, Huang et al. summarized the biomedical applications of melanin/polydopamine (PDA)-based nanomaterials, including bioimaging, treatment, theranostics, antibacterial, UV/radiation protection, biosensor, and tissue engineering [40]. Liu's group highlighted the diverse applications of melanin-like nanomaterials in biological imaging, photothermal therapy, drug delivery for tumor treatment, and other emerging biomedicine-related implementations [21]. Caldas et al. focused on the promising capabilities of melanin/melanin-like nanoparticles regarding optoelectronic, photoconductivity, and photoacoustic [41]. Park and his collaborators briefly reviewed recent approaches in synthesizing melanin-like nanomaterials and their biomedical applications in anti-inflammatory, photothermal therapy, drug delivery, fluorescence-based biosensing, and UV shielding in dermatology [42]. Nevertheless, these kinds of literature rarely involve systematical and comprehensive aspects of natural melanin and melanin-like nanoparticles about applications in imaging-guided disease therapy. Moreover, preparation methods of the nanoparticles mainly refer to the polymerization of synthetic melanin, rarely mentioned melanin nanoparticles originating from organisms. Considering that PDA-based surface-modified nanoparticles have been summarized and discussed in many previous reviews [40,43–47], they will not be presented in detail here. In this review, we mainly focused on the recent progress and design strategies of melanin/melanin-like nanoparticles for application in imaging-guided various diseases therapy (Fig. 1). Firstly, we discuss the preparation of natural melanin/melanin-like nanoparticles, and then highlight their applications in imaging-guided treatment for multiple diseases, including single-modal and multimodal imaging-guided single or synergistic treatment. In addition, the prospects and directions for further development of melanin/melanin-like nanoparticles are discussed, which will be instructive in developing of melanin-based novel therapeutic platforms and clinical translation.

2. Preparation of melanin/melanin-like nanoparticles

Melanin, a natural polyphenolic polymer, widely found in almost all living organisms from bacteria to mammals, is formed by oxidation and polymerization of self-assembling units, such as tyrosine, 3,4-dihydroxyphenylalanine (L-DOPA), and dopamine. Generally, melanin is roughly categorized into five main types based on their structure and monomer precursors: brown-black eumelanin (tyrosine, 5,6-dihydroxyindoles), yellow-reddish pheomelanin (cysteinyldopas, benzothiazines), dark neuromelanin (dopamine, catecholamines), allomelanin (1,8-dihydroxynaphthalene, phenolic precursors) and pyomelanins (homogentisic acid) with eumelanin being the most common one [48–50]. The excellent functionality of melanin is closely related to its unique chemical structure and composition. However, unlike small molecules with defined chemical structures, the molecular structure of melanin is controversial because of its tunable conditions of polymerization [17,51]. To boost the biomedical applications of melanin-based nanomaterials, several challenges must be addressed. Priority should be given to the need to expand the current structure-property-function relationships, which had been reported in some reviews [50,52]. Also, developing new rational methods for solving their source and production problems is equally important. Furthermore, more attention needs to be paid to the pharmacological activity of melanin and its nanoparticles, which will be beneficial in designing new strategies for the treatment of various diseases [53–56]. In general, melanin/melanin-like nanoparticles are obtained by two main methods, extraction and synthesis.

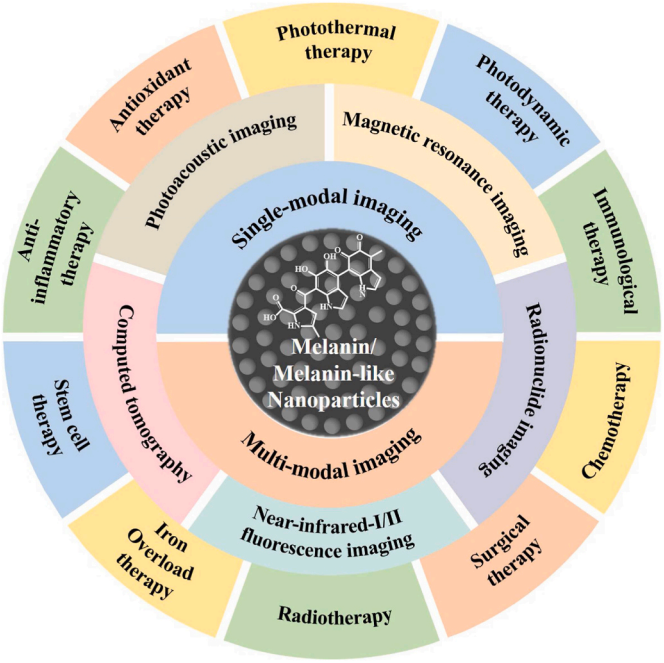

Fig. 1. Schematic illustration of the main imaging-guided disease therapy based on melanin/melanin-like nanoparticles.

2.1. Extraction of natural melanin nanoparticles

Efforts have been made over the years to extract natural melanin nanoparticles by isolating and purifying pigments from organisms such as bacteria, fungus, plants, animals, and even human hair.

2.1.1. Bacteria and fungi source

Many bacteria and fungi have been identified as having natural melanin-producing abilities. Singla et al. extracted irregular melanin with a yield of ~10 % from the pathogenic black knot fungus apiosporina morbosa via acid-base extraction method [48]. Recently, Hou et al. investigated the therapeutic effects of melanin from auricularia auricula on alcoholic liver damage *in vitro* and in vivo [57]. It is found that auricularia auricula melanin inhibited the expression of CYP2E1 and increased the levels of Nrf2 and its downstream antioxidant

enzymes in mice with alcoholic liver injury. To obtain melanin at a relatively low cost and in a large quantity, Martínez's group showed an alternative to acquiring melanin based on the culture of melanogenic microorganisms [49]. By applying genetic engineering techniques to encode related enzymes or generate novel strains, the productive capacity of melanin could be significantly improved. Escherichia coli being a common recipient cell, Mejía-Caballero et al. obtained a strain with the ability to synthesize catechol melanin from a simple carbon source by integrating the MutmelA gene into the chromosome of Escherichia coli W3110 trpD9923. In addition, Ahn et al. prepared synthetic isomelanins using wild-type Streptomyces glaucescens and recombinant Escherichia coli BL21(DE3) strains [58,59].

2.1.2. Plant source

In the plant world, black sesame melanin (BSM) is a rich and safe source of melanin material, obtained by NaOH solubilization and HCl deposition several times from the skin of black sesame seeds, with strong antioxidant and antinitrosating activities. Chu et al. demonstrated that BSM, a macromolecule containing multiple aromatic rings as well as multiple carboxylic and phenolic hydroxyl groups, can be used for sentinel lymph node (SLN) mapping and cancer therapy [16].

2.1.3. Hair source

Inspired by the hierarchical structures in nature, Zhang's team explored the micro-/nanostructures of human hair-derived melanin by decomposing it into hierarchical microparticles (HMP) and hierarchical nanoparticles (HNP) with the action of base extraction and ultrasonication [60]. As shown in Fig. 2a and b, rod-like or oval-shaped HMP could be found with an average width of around 300 nm and an average length of about 1.2 μm. After ultrasonic dispersion, spherical HNP with an average diameter of 80 nm was isolated from HMP, indicating that HMP was assembled from nanosized HNP. Xiao et al. compared intact true melanosomes (pigment particles composed mainly of true melanin) from four species: squid (Sepia officinalis) ink, crow (Corvus ossifragus) feathers, iridescent wild turkey feathers, and black human hair. It is found that true melanosomes from four species consisted of subunits with a length of 10–60 nm, consistent with results in the human hair and squid ink [61]. *In vitro* experiments of hair-derived melanin showed that HMP and HNP could protect skin from damage by UV light. Moreover, they further evaluated the biomedical potential of HMP in cataract prevention. Microcomputed tomography and intraocular fluorescence microscopy results indicated that warfarin-loaded HMP could rescue venous thrombosis in mice. In addition, HNP modified with tumor-targeting aptamers exhibited significant antitumor effects and inhibited 96.8 % of tumor growth in vivo. In 2020, this team combined natural melanin particles extracted from the hair of yellow race with metal ions to mimic natural enzymes [62]. It was found that different metal-bound melanin nanoparticles exhibit various catalytic activities, which may be used as enzyme alternatives to meet multiple requirements in biomedical applications. However, the variability of hair samples cannot be ignored.

2.1.4. Animal source

In addition to the above sources, natural melanin nanoparticles extracted from the ink sac of cuttlefish (CINP) have also been widely investigated. They are usually produced by washing and centrifuging freshly dissected ink sacs, and the process was repeated six to ten times to remove the water-soluble impurities in the ink. Wang et al. got CINP with diameters of approximately 150–200 nm [64]. Water-soluble squid melanin particles were prepared by ultrasound-assisted degradation method under alkaline conditions [65]. Zhang et al. verified that CINP nanoparticles had good biocompatibility, good tumor-associated macrophages (TAMs) repolarization ability, excellent photothermal conversion, and robust photostability. It can be used as an immunomodulator to repolarize M2 TAMs to anti-tumor M1 phenotype and as a near-infrared (NIR) agent to enable PTT to inhibit tumor growth [66]. A similar result has been reported for M2-to-M1 TAMs repolarization and PTT based on iron-chelated melanin-like nanoparticles [67]. By using the feature of chelating metal ions within the polycatechol frameworks, Liang et al. developed a highly stable Fe-chelated CINP mimetic enzyme with peroxidase-like activity to determine total antioxidant capacity in food systems [68]. The prepared melanin nanoparticles have better reusability and stability than the natural enzyme and have good catalytic activity at high temperatures. In recent years,

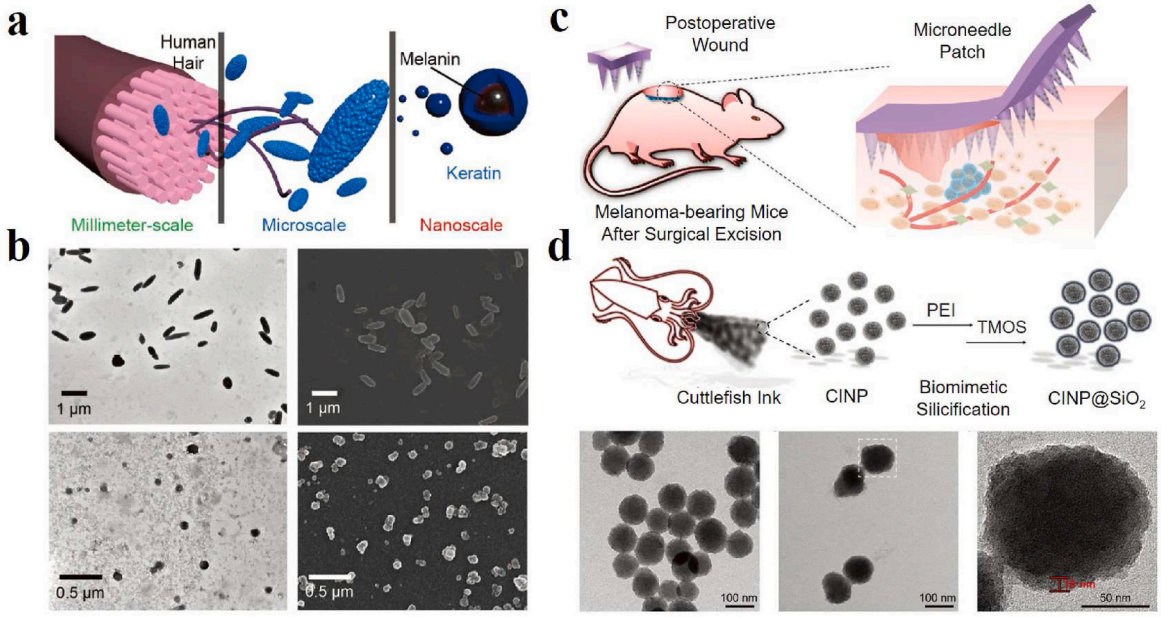

Fig. 2. Case 1: (a) Schematic illustration of the hierarchical micro-/nanostructures from human hair. (b) Transmission electron microscopy (TEM) and scanning electron microscopy (SEM) images of HMP and HNP derived from hair [60]. Reproduced with permission. Copyright 2018, Wiley-VCH. Case 2: (c) Schematic of a microneedle patch loaded with melanin nanoparticles for the treatment of subcutaneous wounds after melanoma surgery. (d) Schematic synthesis process of CINP@SiO_2. TEM images of CINP, CINP@SiO_2, and magnified TEM image of the white dotted box in CINP@SiO_2 [63]. Copyright 2022, Wiley-VCH.

treating multiple diseases based on CINP has become a research hotspot. Araújo et al. used supercritical carbon dioxide to impregnate metronidazole as a model antibiotic drug in spherical CINP. This greatly facilitated pH-targeted therapy of intestinal diseases because of the vital response of melanin to pH and the significant control of drug release [15]. Also, melanin in ink (MSI) could be applied to intestinal diseases due to its anti-inflammatory and antioxidant activities. Oral administration of MSI may modulate TLR4/NF-κB, and NLRP3/ASC/Caspase-1 signaling pathways and reduce the expression of the pro-apoptotic protein Caspase-3, thus increasing the proportion and abundance of dominant bacteria (e.g., Bacillus and Clostridium) to improve inflammatory bowel disease [69]. Based on the antioxidant properties of cuttlefish melanin, Zhou et al. prepared melanin/alginate hydrogels to protect cardiomyocytes from oxidative stress damage and induce anti-inflammatory phenotype (M2) macrophage polarization through PI3k/Akt1/mTOR signaling pathway [70]. Microneedle is considered to be one of the most promising transdermal drug delivery systems. Yu et al. fabricated a hyaluronic acid-based microneedle that encapsulates melanin nanoparticles for both tumor PTT and promotion of skin tissue regeneration (Fig. 2c). The prepared CINP had a homogeneous spherical morphology (Fig. 2d). After encapsulation within an amorphous silica shell, the resulting CINP@SiO_2 showed a rough surface core-shell structure, which can be used as a source of bioactive SiO_4^{4-} to stimulate skin tissue regeneration [63]. In the latest work, Wang et al. developed a yolk-shell nanostructure based on CINP coated with mesoporous SiO_2 [71], which exhibited the synergistic antitumor effect of PTT and thermodynamic therapy upon 1064 nm laser irradiation. Besides, Zynudheen et al. found that melanin extracted from cuttlefish ink has significant photoprotective properties on human hair when exposed to UV radiation [72].

Despite a variety of natural melanin nanoparticles that have been obtained and widely used in the treatments of multiple diseases, complex extraction and purification process, the uncertainty of composition and origin, lack of standardized extraction procedures, high-volume controllable preparation, and other problems limit their further clinical translation. Semi-industrial melanin production using genetic engineering techniques and microbial culture processes is a direction, which could avoid purified tyrosinase, expensive chemical methods, and tedious extraction of polymers from plant and animal tissues [49]. The large size and poor solubility of natural melanin nanoparticles are also obstacles to the application. Fan et al. prepared ultrasmall melanin nanoparticles with high water mono-dispersity, homogeneity, and water solubility by dissolving melanin granules into 0.1 M NaOH solution followed by HCl neutralization assisted by ultrasonication to reduce inter-chain aggregation [35].

2.2. Synthesis of melanin-like nanoparticles

Melanin-like nanoparticles mean artificial synthetic melanin, lacking a few proteins and biomolecules compared with natural melanin nanoparticles. PDA nanoparticles are a kind of the most common melanin-like owing to many similar physical and chemical properties as naturally occurring melanin, which are generated through the oxidation and polymerization of dopamine [41], while the molecular mechanism of dopamine polymerization is still unclear. Presently, it is universally acknowledged that dopamine is oxidized to quinones by the dissolved oxygen in solution, following the formation of 5,6-dihydroxyindole (DHI) resulting from intramolecular cyclization of quinones. Then, two different pathways of covalent oxidative polymerization and non-covalent self-assembly between DHI and dopamine monomer collectively promote the formation of PDA [45,73]. The detailed polymerization mechanism of PDA can be found in previous literature [74,75]. There are two basic methods to prepare PDA nanoparticles: enzymatic oxidation and solution oxidation [21]. Among them, solution oxidation is the most widely used strategy for PDA preparation because it does not require complicated instruments and harsh reaction conditions, and its preparation process is convenient and mild. Under alkaline and aerobic conditions, the polymerization immediately occurs with a change of solution color from colorless to pale brown, and then turning to dark brown. The final PDA nanoparticles were obtained through washing and centrifugation. The morphology, size, yield, and properties of PDA can be well adjusted by controlling the reaction conditions such as time, temperature, concentration, pH, and some additives of the reaction system. In 2011, Ju et al. successfully synthesized a size-controllable melanin-like nanoparticle by NaOH neutralization of dopamine hydrochloride followed by spontaneous oxidation with air, which described good dispersibility and antioxidant activity in the water and biological media [31]. It is reported that polyvinyl alcohol could also control the size and morphology of particles by inhibiting aggregation during synthesis [76]. Wang et al. reported a new method to regulate the size of PDA nanoparticles via adding either potent free radical scavengers (edaravone) or stable free radicals (PTIO•) during the polymerization. The results revealed that edaravone could inhibit the growth of nanoparticles while PTIO• mainly facilitated the seed formation, both resulting in a decrease in the size [77]. Furthermore, various porous melanin nanoparticles have been designed to increase the surface area and enhance the adsorbent properties [78,79]. Besides, a microfluidic technique has been developed in recent years for the production of ultrafast, controlled and monodisperse melanin-like nanoparticles. These particles are generated within seconds in a highly concentrated matrix solution, and the size and morphology of the produced nanoparticles can be precisely manipulated by simply adjusting the parameters of the microfluidic device [80].

In the process of artificial syntheses of melanin-like nanoparticles, additives can be simultaneously incorporated via covalent crosslinking to tune their functions and properties. For instance, Cao and his collaborators developed radical-enriched synthetic melanin by copolymerizing of conventional dopamine monomers with a 4-amino-((2,2,6,6-Tetramethylpiperidin-1-yl) oxyl) TEMPO-coupled L-DOPA. The free radical content was increased by one order of magnitude compared to conventional PDA, and reactive oxygen species (ROS) were effectively eliminated after X-ray irradiation [38]. Similarly, Li's group developed a novel strategy to fabricate melanin-like nanoparticles with controlled size and composition via copolymerization of an essential amino acid and dopamine molecules in an aqueous solution. The disordered non-planar microstructure within the nanoparticles may result in the former being more readily accessible to free radicals, thus exhibiting superior antioxidant properties against cellular oxidative stress [81,82]. Moreover, covalent crosslinking strategies also can adjust the absorption property of PDA nanoparticles. By copolymerization of dopamine and other monomers, the resulting PDA nanoparticles generate the donor-acceptor pairs in the microstructure, which can reduce the energy bandgap and promote the electron delocalization, leading to enhancement of light absorption across a broad spectrum and higher total photothermal effect [83,84]. They also proposed three kinds of metal ion-loaded methodologies: post-doping, pre-doping, and metal ion-exchange strategies to enhance light absorption ability [85].

In addition to PDA-based nanoparticles, other materials can also be exploited as precursors to synthesize melanin-like nanoparticles. For example, a kind of fungal melanin-like, poly-(1,8-dihydroxynaphthalene) nanoparticles (PDHN NPs) with uniform and controllable sizes have been synthesized via a facile ammonium persulfate (APS)- mediated oxidative radical polymerization, which exhibited excellent stability in water and could be used for long-term storage and various biological applications [86]. Zhou et al. reported the artificial allomelanin nanoparticles (AMNPs) via oxidative oligomerization of 1,8-dihydroxynaphthalene using the chemical oxidizing agent sodium periodate ($NaIO_4$) or potassium permanganate ($KMnO_4$). These AMNPs show much higher activity than that of size-matched PDA nanoparticles [87]. Some tripeptides containing tyrosine phenylalanine and aspartic acid can be utilized to synthesize melanin-like nanoparticles by tyrosinase oxidation. Surprisingly, the morphology, functionality, and properties of

these melanin-like peptides also can be tuned [88]. Recently, norepinephrine is recognized as a novel precursor for melanin synthesis. It can undergo oxidative polymerization to form monodisperse nanoparticles and thin coatings [89]. Similarly, Capucciati and collaborators developed water-soluble melanin-protein-Fe/Cu conjugates derived from norepinephrine and fibrillar β-lactoglobulin as an analogue of neuromelanin. The analogue could be applied to the diagnosis of neurodegenerative diseases, including Parkinson's disease and Alzheimer's disease so on [90].

Overall, compared with natural melanin nanoparticles, the size, morphology, microstructure, property, and function of synthetic melanin-like nanoparticles can be precisely regulated by controlling the reaction conditions, showing incredible promise for biomedical application.

3. Imaging-guided therapy of melanin/melanin-like nanoparticles

Biomedical imaging is an indispensable tool in disease diagnosis, intraoperative guidance, and post-surgery evaluation. Currently, numerous imaging technologies have been developed and applied in biomedical and clinical settings, which include magnetic resonance imaging (MRI), computed tomography (CT), single-photon emission computed tomography (SPECT), positron emission computed tomography (PET), NIR-I/II fluorescence imaging (FLI), and photoacoustic imaging (PAI). Among these, PET, SPECT, FLI, and PAI are regarded as quantitative or semiquantitative imaging modalities, whereas CT and MRI are generally used for anatomical imaging.

Nanotheranostics integrate diagnostic and therapeutic agents into one platform. Not only could the location and size of diseased tissues be easily detected before therapy, but also the treatment procedure, pharmacokinetics, and therapeutic effects can be effectively monitored during the treatment [91,92]. The development of multifunctional biomaterials derived from naturally occurring substances in organisms plays a crucial role in medical theranostics, as they can simultaneously fulfill numerous requirements such as natural biosafety, imaging, and therapy, which would be highly beneficial for biomedical applications. Melanin is a well-known biopolymer widely distributed in almost all living organisms and possesses many distinct functions, including excellent biocompatibility and biodegradability, intrinsic PAI property, broadband NIR absorption, high chelating capability to metal ions, unique chemical structures, and so forth. These magnetic properties make melanin/melanin nanoparticles highly intriguing for various biomedical applications, especially for image-guided precise therapy for various diseases, which can monitor pharmacokinetics, biodistribution, and accumulation at the target lesion site. Complex applications in the imaging-guided treatment of melanin-based nanoparticles are discussed in the following.

3.1. Single-modal imaging-guided therapy

Single-modal imaging-guided therapy means using a single imaging method to combine the diagnosis and treatment of disease simultaneously. The use of imaging methods to detect lesions in real-time during treatment allows for the delivery of therapeutic drugs to the right site at the right time and at the right concentration, reducing toxic effects on normal tissue and significantly improving efficacy. Taking advantage of the unique properties of melanin/melanin-like nanoparticles, such as broad optical absorption, strong chelation to various metal ions, and accessible functionalization, they have been widely explored as versatile therapeutic nanoplatforms for single-modal imaging-guided therapy, mainly including PAI, MRI, radionuclide imaging and FLI. Representative examples are shown in Table 1. To further improve the biocompatibility and physiological stability in vivo, Table 2 polyethylene glycol (PEG) molecules containing amino or sulfhydryl groups are frequently used to modify the surface of melanin-based

Table 1
Representative examples of extraction method and application of natural melanin nanoparticles.

Source	Extraction method	Application	Ref.
Pathogenic black knot fungus apiosporina morbosa	Acid-base extraction method	/	[48]
Auricularia auricula	Acid-base extraction method under ultrasonic conditions	Treatment of alcoholic liver damage	[57]
Integrate the gene MutmelA's E. coli W3110 trpD9923	Genetic engineering	/	[58]
Wild-type Streptomyces glaucescens and recombinant Escherichia coli BL21(DE3) strains	Genetic engineering	Cotton fabric dyeing	[59]
Black sesame	Grinding, sieving, washing, dissolving by NaOH, precipitating by HCl, washing with distilled water	Sentinel lymph node mapping and cancer therapy	[16]
Human hair	base extraction and ultrasonication	warfarin-loaded HMP can rescue mice from vein thrombosis tumor targeted aptamers-modified HNP exhibit dramatic antineoplastic effect	[60]
Squid (Sepia officinalis) ink, crow (Corvus ossifragus) feathers, iridescent wild turkey feathers, and black human hair	/	Protect skin from damage by UV light, cataract prevention, antitumor	[61]
Hair of yellow race	Dissolving with NaOH, heating, dialyzing with PBS, and differential centrifugation	Combined natural melanin particles with metal ions to mimic natural enzymes	[62]
Squid	ultrasound-assistant degradation method under alkaline condition	Anti-oxidant activity	[65]
Cuttlefish Ink	differential centrifugation method	Synergizing immunotherapy and PTT to inhibit tumor growth	[66]
Ink sac of cuttlefish	Washing and centrifugation for 6–8 times	Fe-chelated CINP mimetic enzyme with peroxidase-like activity	[68]
Ink sac of cuttlefish	/	Supercritical carbon dioxide to impregnate metronidazole in spherical CINP for pH-targeted therapy of intestinal diseases	[15]
Cuttlefish	Centrifugation method	Protect cardiomyocytes from oxidative stress damage and induce anti-inflammatory phenotype (M2) macrophage polarization	[70]
Ink sac of cuttlefish	Multiple steps of centrifugal washing with deionized water	Tumor PTT and promotion of skin tissue regeneration	[63]
Ink sac of cuttlefish	Differential centrifugation method	Synergistic antitumor effect of PTT/ thermodynamic/ immunotherapy upon	[71]

(continued on next page)

Table 1 (*continued*)

Source	Extraction method	Application	Ref.
Ink sac of cuttlefish	Stirring using 0.5 M HCl and washing with water	1064 nm laser irradiation Photoprotective properties on human hair when exposed to UV radiation	[72]

nanoparticles because these groups can react with dihydroxyindole/indolequinone groups in melanin [35].

3.1.1. PAI-guided therapy

PAI is a hybrid imaging technique that combines optical excitation with ultrasonic detection. During the imaging process, light absorbers in biological tissues generate sound waves once they encounter a laser pulse and are detected by an ultrasound transducer, which is known as the photoacoustic effect. As a non-invasive, radiation-free, novel imaging method, PAI combines the high spatial resolution of ultrasound with the high contrast of optical imaging to a depth of up to 7 cm [121]. Relying on the inherent contrast of tissues (such as endogenous chromophores and melanin), this advanced imaging technology can enhance the imaging effect and achieve real-time, multi-layer, multi-contrast visual dynamic imaging [122]. Moreover, it could provide functional and molecular information through highly specific tissue imaging, thus helping us get non-invasive physiological and pathological imaging at the molecular level in living tissue [123]. Melanin and melanin-like nanoparticles possess intrinsic NIR absorption, making them promising candidates for PAI-guided treatment of multiple diseases.

PAI technology provides a new method for the early detection and treatment of tumors by studying the morphological structure, functional metabolism, physiological and pathological characteristics of biological tissues [124]. For instance, Liu et al. described the water-soluble melanin nanoparticles (MNPs) conjugated with cyclic Arg-Gly-Asp (cRGD) peptides (cRGD-MNPs) to provide preoperative 2D or 3D PA images of tumors for precise surgical resection. The PA intensities of cRGD-MNPs at the tumor site of tumor-bearing mice were significantly higher than that of MNPs [93]. Combined chemo-radiotherapy is one of the most widely applied strategies for clinical cancer therapy. Yi and his collaborators selected copper sulfide (CuS)@Melanin-PEG nanoparticles loaded with doxorubicin (DOX) as the multifunctional therapeutic agent and worked out the general mechanism of increased uptake and decreased outflow of nanoparticles by tumor cells under X-ray irradiation, which is beneficial to in vivo chemo-radiotherapy [94]. Such nanoparticles not only showed strong PA signals but also promoted the apoptosis induced by X-ray as a radiation sensitizer, thus realizing the PAI-guided chemo-radiotherapy. Longo and his partners reported a dynamic contrast-enhanced (DCE)-PA approach to assess tumor vasculature properties and monitor vascular changes following an anti-angiogenic treatment for the first time [95]. Photothermal therapy (PTT) is a promising non-invasive tumor treatment that converts absorbed light into heat by a well-designed photothermal agent to kill tumor cells [125]. Based on their inherent optical absorbance, melanin/melanin-like nanoparticles showed strong potential of PTT in both the visible and the near-infrared regions. PAI-guided PTT is a significant application of melanin and melanin-like nanoparticles in tumor theranostics. In 2017, Yang's group explored red blood cell (RBC) membrane-camouflaged melanin (Melanin@RBC) nanoparticles as a novel PTT platform for in vivo tumor treatment [96]. The platform could effectively evade the reticuloendothelial system recognition, prolong circulation time and improve tumor accumulation. In addition, with the inherited PA property and excellent photothermal conversion ability of cuttlefish melanin nanoparticles, it is desirable for PAI-guided PTT of tumors. Similarly, a work reported that coating of the melanin nanoparticles by the hybrid membrane of RBC and MCF-7 cells had been

Table 2
Representative examples of single-modal imaging-guided therapy based on melanin/melanin-like nanoparticles.

Melanin/melanin-like nanoparticles	Imaging-guided therapy	Cell line *in vitro*	Disease type	Ref.
(cRGD) peptides-conjugated water-soluble MNPs	PAI-guided surgical resection	MDA-MB-231	Tumor	[93]
CuS@Melanin-PEG/DOX	PAI-guided Chemo-Radiotherapy	4T1	Tumor	[94]
Water Soluble Melanin Derivatives	DCE-PAI-monitored antiangiogenic therapy	J774	Tumor	[95]
Melanin@RBC	PAI guided PTT	A549	Tumor	[96]
Melanin@RBC-M	PAI-guided PTT	MCF-7	Tumor	[97]
CuS-Melanin-FA	PAI-guided PTT	4T1	Tumor	[98]
PDA-RGDC/DOX	PAI-guided chemo/photothermal therapy	Hela	Tumor	[99]
M-Dots-CuET	PAI-guided chemo/photothermal therapy	4T1	Tumor	[100]
Melanin-M1	PAI-guided chemo/photothermal therapy	HeLa	Tumor	[101]
MNP-PLL/miR-145-5p	PAI-guided gene/photothermal therapy	Hep-2	Tumor	[102]
Hematoporphyrin-melanin nanoconjugates (HMNCs)	PAI-guided sonodynamic/photothermal therapy	4T1	Tumor	[103]
M@C NPs	PAI-guided photothermal/immune co-therapy	4T1	Tumor	[104]
MIL-100 loading TYR and Tyr	PAI-guided photothermal/chemodynamic combination therapy	4T1	Tumor	[55]
GAGs-PLL-MNP	PAI for monitoring the course of OA progression	/	Osteoarthritis	[105]
Dex-pPADN	PAI-guided anti-oxidation and anti-inflammatory therapy	Raw 264.7, ATCD5	Osteoarthritis	[106]
PADN	PAI-guided anti-oxidation therapy	Raw 264.7, L02	Acute liver injury	[107]
GMP nanoparticles	PAI-guided antioxidant, antiapoptotic, and anti-inflammatory therapy	NRK-52E	Acute kidney injury	[108]
PDA nanoparticles	PAI-guided anti-inflammatory therapy	Raw 264.7	Acute peritonitis and acute lung injury	[109]
Mn^{2+}-chelated PDA Nanoparticles	MRI guided PTT	4T1	Tumor	[110]
PDA-ICG-PEG/DOX (Mn)	MRI guided chemo- & photothermal combination therapy	4T1	Tumor	[111]
Alendronate-conjugated PDA	MRI guided chemo-	NIH 3T3,	Tumor	[112]

(*continued on next page*)

Table 2 (*continued*)

Melanin/melanin-like nanoparticles	Imaging-guided therapy	Cell line *in vitro*	Disease type	Ref.
nanoparticle loading SN38 (PDA-ALN/SN38)	photothermal treatment	MSCs, MDA-MB-231, PC-9		
Mn^{2+}-doped melanin-like nanoparticles-PheoA	MRI guided photodynamic therapy (PDT)/ PTT combination therapy	HCT 116	Tumor	[113]
Fe(III)-chelated PDA nanoparticles	MRI guided PTT/ immunotherapy	4T1	Tumor	[114]
^{64}Cu-PEGMNPs	PET/CT-guided radionuclide therapy	A431	Tumor	[115]
^{89}Zr-MNPs	PET-guided iron overload therapy	NIH-3T3	Iron overload	[116]
MNP-Ag-^{131}I	SPECT and Cherenkov radiation imaging-guided radiotherapy	PC3	Tumor	[117]
Cy5.5-labeled P/T@MM	PTT and tumor-associated macrophages repolarization	4T1	Tumor	[118]
Fe^{II}PDA@IR780PEG-cRGD	Ferroptosis	B16F10	Tumor	[119]
DOX/HCuS@PDA-MB	FLI-guided chemo/ photothermal therapy	MDA-MB-231	Tumor	[120]

produced for enhancing therapeutic efficacy in MCF-7 tumor-bearing nude mice (Fig. 3a) [97]. After intravenous injection of Melanin@RBC-M with the size of 124 nm into MCF-7 tumor-bearing mice, PA results revealed distribution, metabolism, and removal of Melanin@RBC-M nanoparticles from the tumor sites (Fig. 3b). Interestingly, the platform exhibited prolonged blood circulation and homotypic targeting to source MCF-7 cells simultaneously. Besides, in vivo results revealed that the Melanin@RBC-M with a 1:1 membrane protein weight ratio of RBC to MCF-7 showed the best efficiencies in tumor inhibition (Fig. 3c and d). For more effective PAI to guide PTT, Qi et al. reported a biomimetic approach to synthesize folic acid (FA) modified CuS nanodots by using melanin as a biotemplate and FA as a stabilizer. The as-prepared CuS-Melanin-FA composite nanoprobes with high near-infrared absorption are promising for PAI and PTT on 4T1 tumor-bearing mice [98].

The PTT is usually combined with other therapies to achieve synergistic effects [126]. Arginine-glycine-aspartic-cysteine acid (RGDC) peptide-modified PDA nanoparticles loading DOX were developed for both the controlled release triggered by NIR light, and pH dual-stimuli and PAI-guided chemo-photothermal synergistic therapy of tumor [99]. In another work, copper(II) diethyldithiocarbamate complex (CuET), as the main component of disulfiram, has been loaded with melanin nanoparticles (M-Dots) through hydrophobic interaction. The final nanoparticles showed good tumor accumulation, as evidenced by the enhanced PA signals in tumor regions, and the tumor growth inhibition value reached 45.1 % [100]. Similarly, Pt(II)-based metallacycles also are loaded with melanin nanoparticles for precisely PA imaging-guided chemo-photothermal combinational therapy [101]. It is reported that PTT can enhance gene therapy efficacy by enhancing the tumor cell uptake of genes and accelerating gene release from nanocarriers. Fan et al. raised a PAI-guided anticancer strategy based on poly-L-lysine functionalized melanin nanoparticles to deliver miR-145-5p mimics (MNP-PLL/miR-145-5p) [102]. By integrating thermo-gene therapies into one theranostic nanoplatform, the nanoparticles significantly depleted the metastatic potential of tumor cells and suppressed the progression of laryngeal squamous cell carcinoma. Besides, Zhang and co-workers prepared the

Table 3
Representative examples of dual-model imaging-guided therapy based on melanin/melanin-like nanoparticles.

Melanin/melanin-like nanoparticles	Imaging-guided therapy	Cell line *in vitro*	Disease type	Ref.
MNP-Mn	MRI/PAI guided PTT	Hep-2, NIH 3T3	Tumor	[149]
Lip-Mel	MRI/PAI guided PTT	MDA-MB-231	Tumor	[150]
PPBR	MRI/PAI guided autophagy promotion-associated PTT	NIH3T3, Hela, MDA-MB-231	Tumor	[151]
OBX-MMNs	MRI/PAI guided mild hyperthermia-enhanced chemotherapy	MDA-MB-231, MDA-MB-468	Tumor	[152]
IR820-PEG-MNPs	PAI/MRI guided selective ablation	HepG2, Huh7	Tumor	[153]
ANG-MnEMNPs-Cur (AMEC)	MRI/PAI guided antioxidation and anti-neuroinflammation	bEnd. 3	Traumatic Brain injury	[154]
SRF-MNPs	PAI/PET-guided chemotherapy	NIH 3T3, HepG2	Tumor	[28]
MNP-PEG-H2	NIR-II FLI/PAI tracking hUMSCs and liver regeneration therapy	hUMSCs	Acute liver injury	[155]
Pt(II) metallacycle/ NIR-II molecular dye/ melanin dots	NIR-II/PAI guided chemo-PTT therapy	U87MG	Tumor	[156]
Gd-Mel@SiO_2	MRI/FI guided PTT therapy	PC-3	Tumor	[157]
Mn^{2+}-chelated melanin nanoparticles (MMMP)	PET/MRI guided antioxidant therapy	HEK293	Acute kidney injury	[158]
CH-4T/ SLB–MSN–Mdot /$^{64}Cu^{2+}$	NIR-II FL/PET guided surgery	NIH3T3, A431	Tumor	[159]

Table 4
Representative examples of tri-modal imaging-guided therapy based on melanin/melanin-like nanoparticles.

Melanin/melanin-like nanoparticles	Imaging-guided therapy	Animal Model	Disease type	Ref.
^{64}Cu-magnetic melanin nanoparticles (^{64}Cu-MMNs)	PET/MRI/PAI guided PTT	U87MG	Tumor	[168]
Core-Satellite Polydopamine-Gadolinium-Metallofullerene	PET/MRI/PAI guided chemo-photothermal therapy	U87MG	Tumor	[169]
GNR@MNP-Gd-^{64}Cu	PAI/PET/MRI guided PTT	Hep-2	Tumor	[170]
Au-decorated melanin (Au-M) nanocomposites	CT/PAI/thermal imaging guided PTT	4T1, HUVEC	Tumor	[171]
RMDI	FLI/MRI/PAI guided photothermal-enhanced chemotherapy	U87MG	Tumor	[172]
Ce6@$CaCO_3$-PDA-PEG	FLI/MRI/PAI guided PDT	4T1	Tumor	[173]
PMNs–II–813	PET/MRI/PAI-guided radioisotope therapy (RIT) and PTT	LNCaP, PC-3	Tumor	[174]

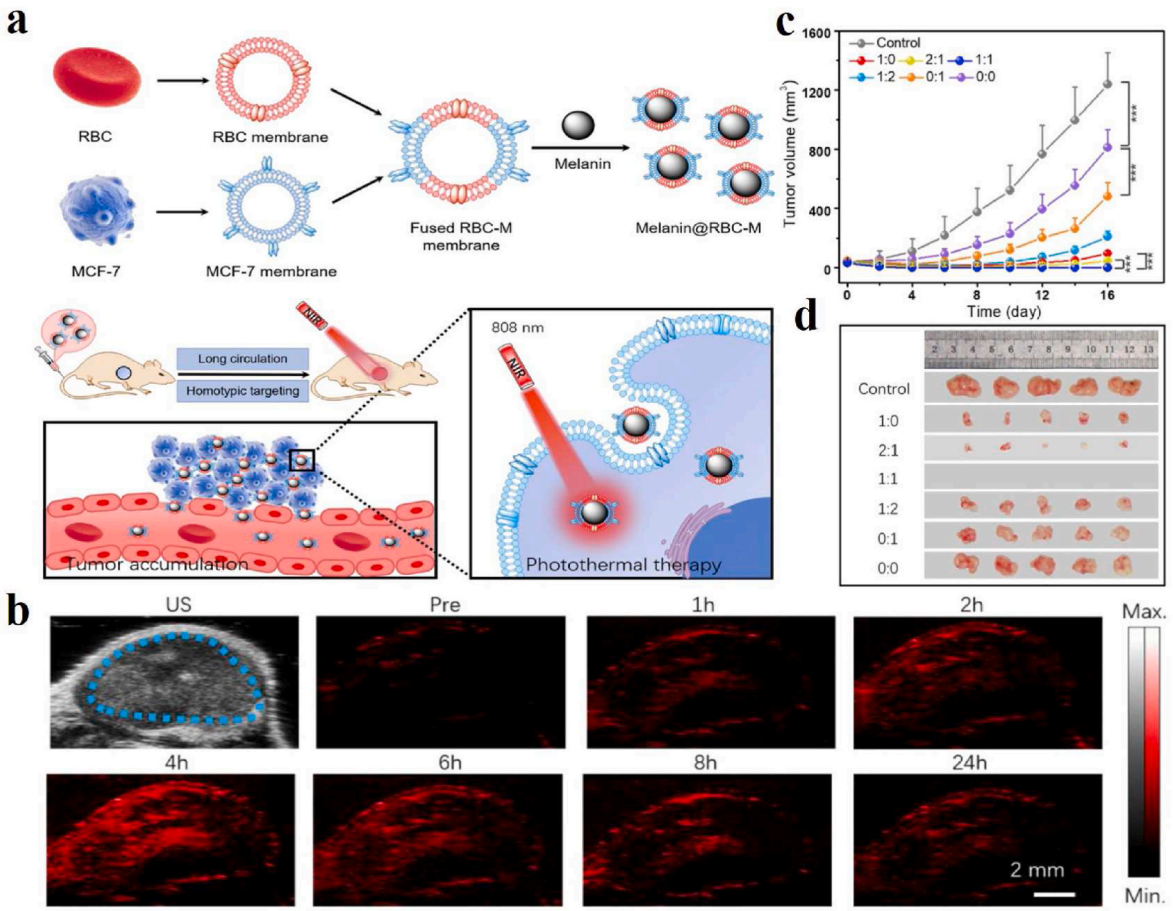

Fig. 3. (a) Schematic illustration of erythrocyte-cancer cell hybrid membrane-melanin (Melanin@RBC-M) nanoparticles with long circulation and homotypic targeting for efficient PTT in tumors. (b) PA images of tumor regions at different time points before (Pre) and after intravenous injection of 0.1 mg of Melanin@RBC-M in MCF-7 tumor-bearing mice. Blue dashed lines point out the tumor regions. Tumor growth curves (c) and excised tumor photos (d) of MCF-7 tumor-bearing mice after PTT treatment at 4 h after intravenous injection of Melanin@RBC-M with different membrane protein weight ratios of RBC to MCF-7 (1:0, 2:1, 1:1, 1:2, 0:1, and 0:0) [97]. Copyright 2019, Elsevier. (For interpretation of the references to color in this figure legend, the reader is referred to the Web version of this article.)

hematoporphyrin-melanin nanoconjugates (HMNCs) with the hematoporphyrin fraction derived from haemoglobin for sonodynamic therapy (SDT) and the melanin fraction derived from cuttlefish ink for PTT. Upon intravenous injection, HMNCs could be aggregated in the tumor region, providing high contrast for tumor PA and thermal imaging, and the SDT-PTT synergy significantly inhibited tumor growth compared to SDT or PTT alone [103]. Recently, Li et al. developed a PAI-guided photothermal and immune co-therapy strategy for treating breast cancer based on cuttlefish melanin nanoparticles coated with a cancer cell membrane (M@C NPs) to achieve homologous adhesion of tumors. The M@C NPs acted as the PTT agent for enhanced antitumor immune response by inducing immunogenic cell death [104]. Inspired by endogenous biocatalytic reactions, Chen's group developed a tumor-specific imaging-guided combination therapy strategy that triggers the biocatalysis of tyrosinase (TYR) and tyrosine (Tyr) through the tumor microenvironment to produce endogenous melanin [55].

PAI-guided antioxidant and anti-inflammatory treatments based on melanin/melanin-like nanoparticles are also a research hotspot in recent years because of their good biocompatibility and natural antioxidant capacity. For instance, Chen's group investigated the feasibility of PAI applied for monitoring the course of osteoarthritis (OA) progression in vivo via anionic glycosaminoglycans (GAGs)-targeted nanoprobe [105]. Positively charged poly-L-Lysine-melanin complexes (PLL-MNP) can be combined with anionic GAGs in cartilage through electrostatic attraction. The PAI results indicated that the contents of GAGs in vivo steadily decreased from the development of OA initial stage to the endpoint of the investigation. Recently, Zhao et al. reported a novel strategy to mimic in situ melanin formation by developing a PEGylated, phenylboronic-acid-protected L-DOPA precursor (PAD) that can self-assemble into well-defined nanoparticles (pPADN) and load with dexamethasone (Dex) for the treatment of OA (Fig. 4a) [106]. TEM and dynamic light scattering (DLS) measurements revealed that the morphology of Dex-pPADN is a homogeneous spherical structure and the hydrodynamic diameter was approximately 89.6 nm (Fig. 4b). The pPADN was converted to PEG-L-DOPA in an oxidative microenvironment due to the deprotection of phenylboronic acids. Then the PEG-L-DOPA was oxidized and polymerized into an antioxidative melanin-like structure by the biosynthetic pathway. At the same time, the structural transformation of pPADN triggers the specific release of Dex. As shown in Fig. 4c, the PA signals of Dex-pPADN showed an increase in $ONOO^-$ concentration-dependent manner. The experiment in vivo as shown in Fig. 4d–g, the intensities of PA signals gradually increased over time in the knee joint of the OA model group. Only a slight enhancement of PA signals was observed after pPADN or Dex-p treatment. Especially, the PA signal in the knee area after Dex-pPADN treatment was lower, similar to that in the healthy group. Overall, these results indicated that Dex-pPADN showed a good therapeutic effect for OA in a rat model by synergetic anti-oxidation and anti-inflammatory effects. PAI signal activation by ROS helped guide therapy. In the same year, they also confirmed that PADN could be used to monitor via ROS-activated PA imaging noninvasively and treat the acute liver injury in mice [107]. Melanin and melanin-like nanoparticles can also be used for other

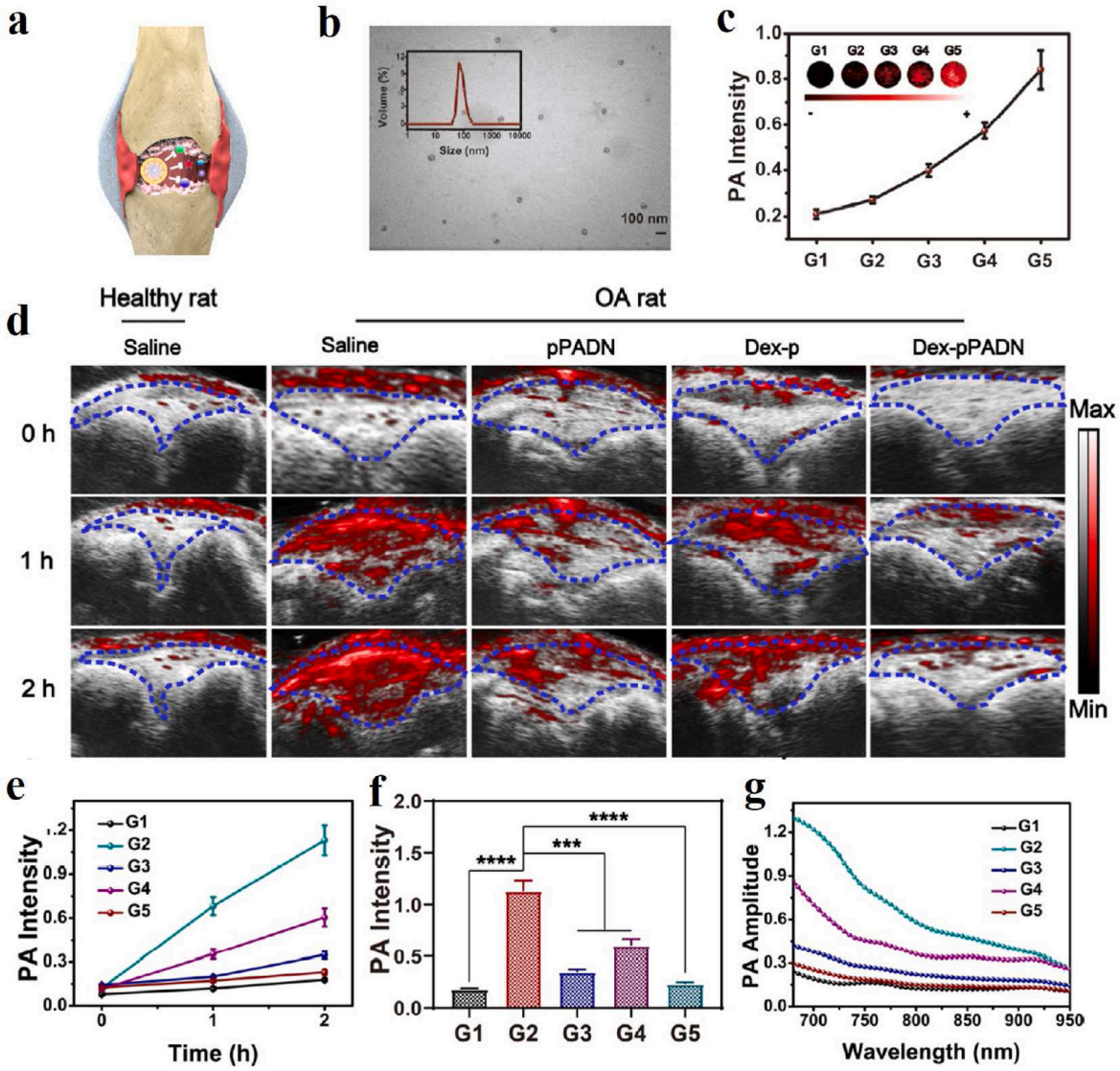

Fig. 4. (a) Schematic illustration of Dex-pPADN for treatment of osteoarthritis. (b) TEM image and hydrodynamic diameter distribution of Dex-pPADN at the pPAD/Dex ratio of 10:1. (c) PA signal intensity and images of Dex-pPADN after incubation with different concentrations of $ONOO^-$ (G1: 0 mM, G2: 5 mM, G3: 10 mM, G4: 20 mM, G5: 40 mM). (d) Representative PA images of a healthy articular cavity or an arthritic articular cavity with different treatments at 0, 1, and 2 h. (e) PA signal intensity of Dex-pPADN at various time points in different groups. (f) PA signal intensity of Dex-pPADN at 2 h in different groups. (g) PA spectra of Dex-pPADN at 2 h in different groups [106]. Copyright 2021, Wiley-VCH.

oxidative stress-related diseases. Our group developed a targeting nanodrug delivery platform for treating rhabdomyolysis-induced acute kidney injury (AKI) under PAI monitoring in mice (Fig. 5a) [108]. The platform was constructed by loading inhibitor PJ34 with anti-GRP97 coupled-melanin nanoparticles (GMP nanoparticles). As shown in Fig. 5b, PA images of mouse kidneys showed increased signal after intravenous injection of GMP nanoparticles. Over time, they peaked after 6 h due to the targeted accumulation of GMP nanoparticles, which promotes the GMP nanoparticles to exert their multiple regulatory effects to alleviate AKI. By measuring blood oxygensaturation (SaO_2) and hemoglobin content (HbT) according to PAI, the results indicated that the serum levels of SaO_2 and HbT in the treatment group were significantly higher than those in the AKI group, which visually confirmed the therapeutic effect of GMP nanoparticles in vivo (Fig. 5c). Besides, PDA nanoparticles have been reported by Zhao et al. for treatment of the acute inflammation-induced injury [109]. It is demonstrated that 80 nm-sized nanoparticles efficiently scavenged either hydrogen peroxide (H_2O_2) or lipopolysaccharide (LPS)-induced cellular ROS *in vitro*, and confirmed the successful suppression of in vivo inflammation in murine acute peritonitis models.

In addition to the applications listed above, Lin et al. used cuttlefish melanin nanoparticles as a periodontal PA probe to estimate the detection depth in the porcine model [127]. Recently, a great deal of work also focused on enhancing the PA properties of melanin. Ju et al. present pH-responsive melanin-like nanoparticles (MelNPs) by modifying the surface of bare MelNPs with hydrolysis-susceptible citraconic amide. After exposure to mildly acidic conditions, the MelNPs became aggregated, and the PA signal was 8.1 times stronger than under neutral conditions [128]. In a similar principle of aggregation, Yim et al. reported PDA nanocapsules loaded with small molecular dyes for enhanced PA-mediated heparin detection to avoid bleeding complications associated with anticoagulant therapy via heparin-mediated disassembly or aggregation [129]. Apart from using the strategy of self-assembly aggregation, gold, and silver nanoparticles have been used for substantial PA signal enhancement [130,131]. Although melanin or melanin-like nanoparticles have made some progress as PA contrast agents for in vivo imaging of animals, the construction of degradable or metabolizable melanin-based nanoparticles is necessary, especially

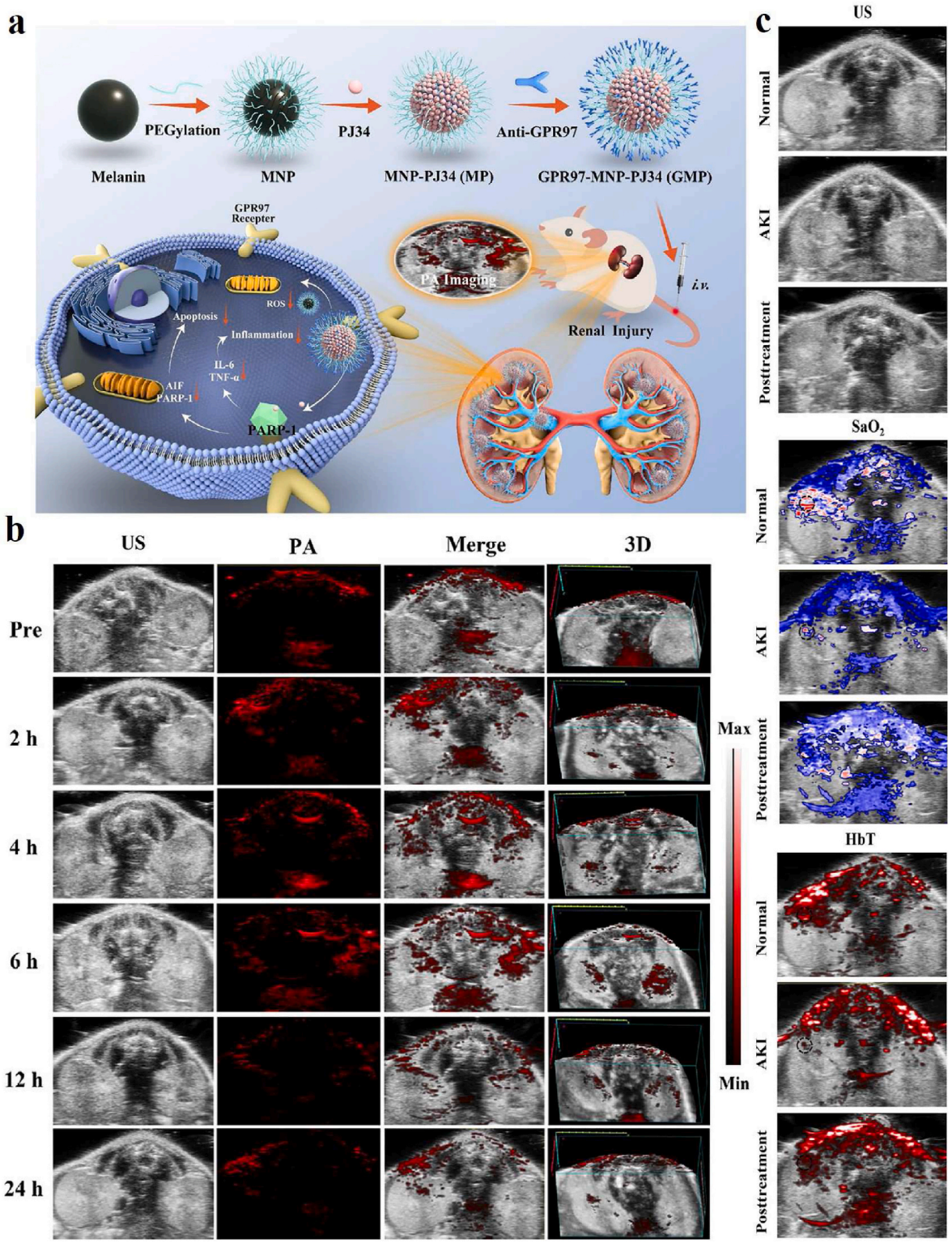

Fig. 5. (a) Schematic of GMP nanoparticle preparation and its PAI-guided antioxidant, anti-apoptotic and anti-inflammatory synergistic treatment of rhabdomyolysis-induced AKI. (b) PA images of AKI mice at different time points after intravenous injection of GMP. (c) Distribution of SaO_2 and HbT in normal, AKI and GMP-treated groups [108]. Copyright 2022, Elsevier.

having in mind clinical applications.

3.1.2. *MRI-guided therapy*

MRI utilizes certain nuclei in the body's tissues, and the resulting radiofrequency signals are processed by an electronic computer, which ultimately allows for the reconstruction of a series of images of a particular layer of the body. Over the past few years, MRI has become one of the most prominent clinical imaging techniques, providing precise anatomical and physiological information with high spatial and temporal resolution and no depth limitations [92]. Although some progress has been made in the exploitation of MR contrast agents, further efforts are needed to increase contrast, biodegradability, and

biosafety. Therefore, the development of MRI contrast agents composed of naturally occurring components in organisms is of high benefit for advanced biomedical applications. As a natural polymer with both biocompatibility and biodegradability, melanin-based nanoparticles have attracted extensive attention as MRI contrast agents due to their strong metal ions chelation with the widely existing phenolic hydroxyl group. In general, three strategies have been used to prepare melanin-based nanoparticles containing metal ions, mainly including post-doping, pre-doping, and metal ion-exchange. (1) Most melanin nanoparticles bind metal ions via a post-doping strategy. For instance, Lee and his copartners introduced one synthetic melanin-like nanoparticle and then functionalized them with biocompatible PEG units and chelated them with paramagnetic Fe^{3+} ions, which can be used as a contrast agent for T1-MRI [132]. By chelating paramagnetic metal ions with PEG-modified ultrasmall melanin nanoparticles, our group successfully constructed a tumor-targeting T1 MRI contrast agent and realized the real-time tracing of stem cells in vivo, including cellular viability, biodistribution, differentiation capacity, and long-term fate [133–136]. Furthermore, we investigated the binding properties of melanin toward various metal cations (Gd^{3+}, Mn^{2+}, Fe^{3+}, and Cu^{2+}), and compared their MRI contrast enhancement effects in different metal-chelated forms *in vitro* and in vivo [24]. (2) The pre-doping strategy has also been adopted for the synthetic melanin-like particles containing metal ions. Li et al. prepared Fe^{3+}-chelated PDA for MRI through a pre-doping strategy, which employs a mixture of Fe^{3+}-(dopamine)$_3$ and free dopamine as the precursor. The doping levels of Fe^{3+} inside the particle are higher and tunable compared with PDA-Fe^{3+} fabricated via post-doping strategy so that it is suitable for MRI [137]. In the following work, Chen's group also used this strategy to prepare the manganese-eumelanin coordination nanocomposites (MnEMNPs), in which 3,4-dihydroxy-DL-phenylalanine (DL-DOPA) served as a precursor and $KMnO_4$ is used as the Mn source and an oxidant (Fig. 6a). MnEMNPs with high-performance longitudinal-transverse (T1-T2) dual-modal magnetic resonance imaging showed significant concentration dependence in both T1-weighted imaging (T1WI) and T2-weighted imaging (T2WI) at different magnetic fields, and the r1 and r2 relaxation rates were obtained from the slopes (Fig. 6c–e) [138]. Besides, the MnEMNPs solution also showed remarkable concentration-dependent PA signals (Fig. 6b). (3) Metal ion-exchange strategy: Jokerst's team obtained Gd^{3+}-loaded synthetic melanin nanoparticles via polymerization of L-DOPA and dopamine in the presence of Mn^{3+} and then displaced the Mn^{3+} from with Gd^{3+}, which showed higher PA intensities so that it can be applied for PA and MR dual-modality imaging [139]. In 2017, a similar method of generating gadolinium-polydopamine nanoparticles (GdPD-NPs) with tunable metal loadings and high relaxivities (a relaxivity of 75 and 10.3 mM^{-1} s^{-1} at 1.4 and 7 T, respectively) were reported [140], which exhibiting great promise in tumor MR imaging.

Through coordinating transition metal ions with catechol groups, metal-melanin nanocomplexes can be established and employed for MRI-guided therapy to augment the diagnostic specificity and accuracy [114]. PEGylated Mn^{2+}-chelated PDA nanoparticles (PMPDA NPs) have been successfully developed in Xu's group as novel theranostic agents without the assistance of any extrinsic chelators. The as-prepared PMPDA NPs showed excellent abilities of simultaneous MRI signal enhancement and photothermal ablation of cancer cells [110]. Dong et al. exploited a versatile nanoplatform based on PDA loading indocyanine green, DOX, and Mn^{2+} for MR imaging-guided combined chemo- & photothermal therapy with minimal side effects [111]. In 2018, the alendronate-conjugated polydopamine nanoparticle (PDA-ALN) loading drug SN38 was successfully developed for the bone-targeted chemo--photothermal treatment of malignant bone tumors [112]. The nanoparticles exhibited excellent photothermal effects and high affinity to hydroxyapatite. MRI in vivo indicated more PDA-ALN accumulated at the osteolytic bone lesions in the tumors compared with the non-targeting PDA. Finally, the combined chemo-photothermal therapy efficiently suppressed the growth of bone tumors and reduced the osteolytic damage of bones at a mild temperature of around 43 °C. Besides, Mn^{2+}-doped poly(L-DOPA) nanoparticles designed by Yang's group exhibit excellent π-π stacking, drug loading, NIR and glutathione dual-stimuli-responsive drug release, photothermal and photodynamic therapeutic activities, and T1-positive MRI contrast, and can serve as a multifunctional nano-platform for cancer therapy [113]. Metal-melanin

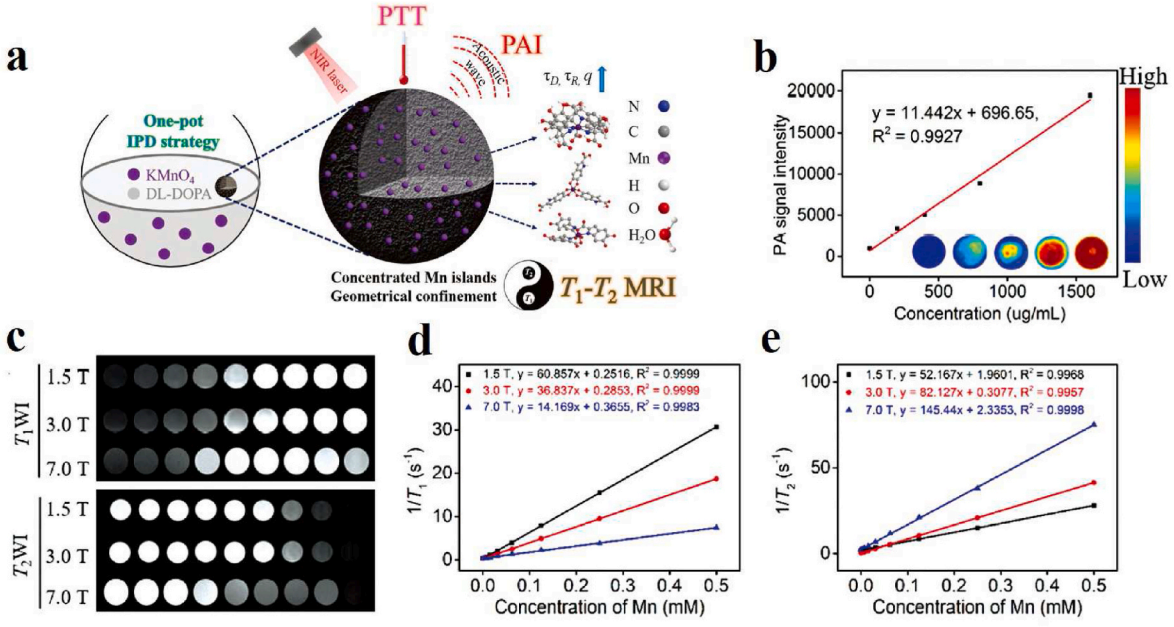

Fig. 6. (a) Schematic illustration of manganese-eumelanin nanocomposites preparation by one-pot method and their T1-T2 bimodal MRI and PAI-guided tumor PTT. (b) PA images of MnEMNPs with different concentrations under 800 nm and their signal intensities as a function of concentration. (c) T1WI and T2WI MR images of MnEMNPs at different Mn ion concentrations and different field strengths. (d) Linear relationship between Mn ion concentrations and r1 relaxation rate in MnEMNPs at different field strengths. (e) Linear relationship between Mn ion concentration and r2 relaxation rate in MnEMNPs at different field strengths [138]. Copyright 2018, Wiley-VCH.

nanocomplexes enable not only MRI but also the locally released metal ions can play an important role in antitumor treatment in vivo. Recently, Yin and his group described one Fe^{3+}-chelated PDA (Fe-PDA) nanoplatform through a prechelation-polymerization strategy (Fig. 7a) [114]. On the one hand, Fe-PDA nanoparticles displayed the T1-weighted MRI contrast enhancement both *in vitro* and in vivo (Fig. 7b–d). On the other hand, the Fe ions existing in Fe-PDA were able to greatly increase the light absorption of PDA in NIR region, resulting in a superior PTT effect. Furthermore, these Fe-PDA nanoparticles could release Fe ions in the tumor environment through the ability of H_2O_2 response, activating an antitumor immune response upon polarizing macrophages toward the M1 mode. Therefore, the design of Fe-PDA nanoparticles has inspired melanin-based materials in imaging-guided tumor suppression.

3.1.3. *Radionuclide imaging-guided therapy*

Radionuclide imaging is currently the most widely used and mature molecular imaging technique. After a radiopharmaceutical enters the human body, radionuclide imaging can capture images based on the difference in uptake of the radiopharmaceutical inside and outside the organ or between normal and diseased tissues, and has the characteristics of high sensitivity (picomolar) and precise quantification, which helps to measure biological processes at the molecular and metabolic levels in vivo. Among radionuclide imaging techniques, PET is the most widely used in scientific research [141]. Conventional imaging techniques only show disease-induced changes in anatomical structure, while PET can reveal changes in the physiological functions of the subjects. Moreover, PET can also provide information on the kinetics, dosimetry, and distribution of drugs in the diseased and normal tissues

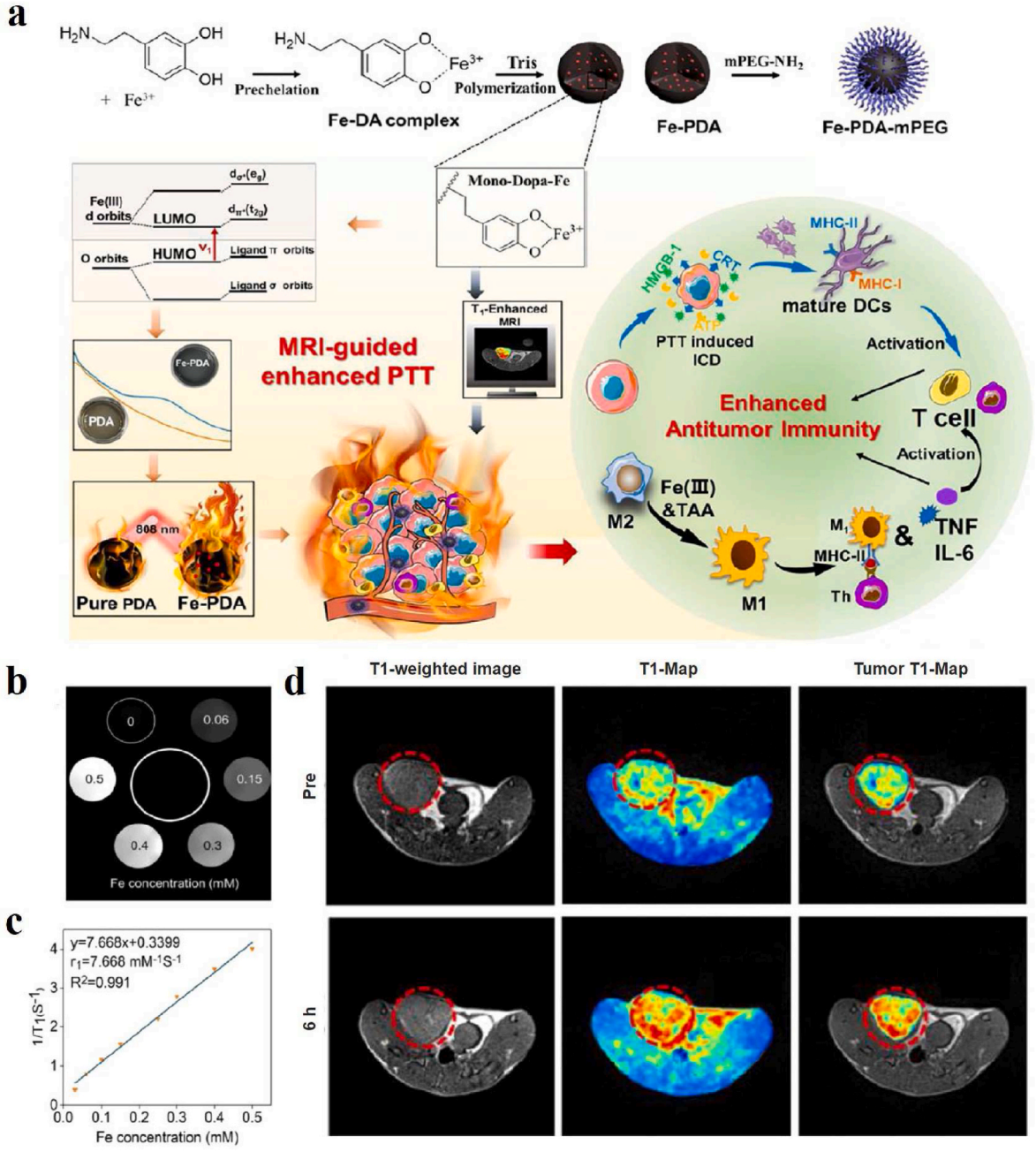

Fig. 7. (a) Schematic representation of Fe-PDA-mPEG NPs synthesis, MRI-mediated enhanced tumor PTT, and triggered anti-tumor immune activation in vivo. (b) T1WI images of Fe-PDA in water with different iron ion contents. (c) Linear relationship between Fe ion concentrations and r1 relaxation rate. (d) T1WI images of tumor-bearing mice in vivo before and 6 h after intravenous injection of Fe-PDAmPEG NPs [114]. Copyright 2022, American Chemical Society.

within the field of view, as well as the clearance pattern in a biological system, which is crucial for understanding drug action and establishing dosage regimens and treatment strategies. Due to inherent chelating abilities to positron-emitting radionuclides such as ^{64}Cu, ^{68}Ga, or ^{89}Zr, the melanin and melanin-like nanoparticles could be employed for PET imaging and imaging-guided therapy. Recently, Zhou et al. prepared ^{64}Cu-labeled PEGylated melanin nanoparticles (^{64}Cu-PEGMNPs), and to further realized the integration of tumor diagnosis and treatment on the A431 tumor-bearing mice [115]. Small-sized melanin nanoparticles have deep penetration in tumors, while their retention in the tumor is not ideal, because they continue to backflow into the blood or are cleared into the surrounding tissues. In light of this, Lan et al. reported pH-responsive melanin nanoparticles by introducing a hydrolysis-susceptible citraconic amide on the surface. After intravenous injection, the nanoparticles entered the tumor with acidic pH, and the electrostatic attractions between nanoparticles drove nanoparticle aggregation and size increase, resulting in enhanced accumulation in the tumor site. Moreover, ^{68}Ga-labeled melanin nanoparticles exhibited enhanced PET imaging [142].

Melanin, as an endogenous iron chelator, accomplishes better therapeutic effects on iron overload diseases. Yang et al. first proposed the discovery of an efficient iron-removal nano-drug based on the native biocompatibility and metal-chelating character of melanin nanoparticles (MNPs) [116]. The ultrafine size combined with polyethylene glycol and considerable metal-binding sites leads to long cycle times and high iron catches. Meanwhile, the blood circulation of PEG-MNPs can be monitored by simple chelation to ^{89}Zr through PET imaging. Compared with traditional drug deferoxamine, MNPs exhibited superior therapeutic effects of iron excretion and a favorable safety profile. In order to study the pharmacokinetics of water-soluble melanin nanoparticle (MP) in iron overload mice, they also developed a simple and rapid method by chelating MP with ^{89}Zr, exhibiting a high yield and excellent stability [143]. Biodistribution studies and MicroPET imaging suggested that ^{89}Zr-MP was mainly distributed in the organs of iron overload and predominantly hepatic excretion. The favorable pharmacokinetics and specific hepatic targeting hold promise for the development of melanin-based nanodrug for iron overload. Besides, Sheng et al. developed a radioiodine-labeled melanin nanoparticle (MNP-Ag-^{131}I) through a novel Ag–I two-step method, which was used for SPECT, Cherenkov radiation imaging, and brachytherapy [117].

3.1.4. FLI-guided therapy

FLI is an advanced technique that utilizes the special properties of fluorescent probes for imaging. Relying on fluorescent probes to label samples, the excited fluorescent substances emit fluorescence at special wavelengths, and these fluorescence can be converted into electrical signals or images, which are then displayed on a computer screen. As a non-invasive and most widely adopted imaging technique, NIR FLI can visualize biological processes occurring in living organisms, and is characterized by high sensitivity, high specificity, and ease of operation. The chemical conjugation or physical absorption of small-molecule fluorescent dyes is the most commonly used method for labeling melanin and melanin-like nanoparticles. Zhao et al. combined Cy5.5 molecules with macrophage membrane-coated PDA nanoparticles carrying repolarization agent (P/T@MM) in 4T1 tumor-bearing mice to investigate whether macrophage membrane artifacts could deliver the expected targeting to post-PTT tumor tissues in vivo [118]. In the following study by Luo's group, a small fraction of Fe^{II}PDA@IR780-PEG-cRGD nanoparticles administered to mice was trapped in the liver and kidney. The biodistribution also showed that the nanoparticles accumulated to a maximum of about 8 h after administration. After modification with hydrophilic PEG1500, it was demonstrated that a hydrated layer on the nanoparticle surface was formed for spatial stabilization, thus avoiding mononuclear phagocyte system trapping and scavenging, facilitating the photothermal response of the iron-chelating biopolymer nanoplatforms to activate iron deposition in target tumor cells remotely [119]. In addition, a PDA-engineered nanobeacon DOX/HCuS@PDA-MB (D/CP-MB) for tumor-associated HSP90 fluorescence detection and NIR-triggered drug release reconnaissance was developed for sensitized chemotherapeutic-PTT therapy. With the help of NIR and the guidance of fluorescence imaging, the spatiotemporal release of DOX can be achieved by triggering the photothermal effect, thus enabling combined chemotherapy and photothermal therapy [120]. Apart from FLI-guided tumor therapy, Yang et al. demonstrated the feasibility of PDA nanoparticles as potent antioxidants in a mouse periodontitis model (Fig. 8) [144]. As shown in Fig. 8a and b, monodisperse spherical PDA nanoparticles with an average diameter of 160 nm were well generated by self-polymerization at room temperature, which can effectively remove reactive oxygen species. In more detail, the high fluorescence signal in Fig. 8c was detected around the DCFH-DA injection site in the LPS-treated group due to the existence of local inflammation. However, almost no fluorescence signals were found in the control group or the PDA NPs-treated group, confirming the alleviation of periodontal inflammation.

In recent years, the newly emerging NIR-II FLI technology has been widely used in the field of biological imaging in vivo. Compared with conventional NIR-I imaging (700–950 nm), NIR-II imaging (950–1350 nm) greatly improves imaging resolution and depth because at longer wavelengths, photon scattering is reduced and the auto-fluorescence background is lowered, so NIR-II imaging can visualize deeper anatomical structures [145–147]. Based on these advantages, a NIR-II dye-labeled natural cuttlefish melanin nanoprobe developed by Dong et al. not only improve the water solubility and biocompatibility and prolong the retention time of small molecule dyes but realize the preoperative and intraoperative assessment of lymphatic metastases [148].

3.2. Dual-model imaging-guided therapy

In the past few years, tremendous advances in single-modal imaging have been applied for preclinical applications, yet each imaging modalities possess its own merits and drawbacks. For instance, MR and CT imaging are the most common clinical imaging techniques that provide a high spatial resolution of biological tissue, while with poor sensitivity. SPECT and PET possess a series of advantages, including high sensitivity, unlimited penetration depth, and quantifiable results, unluckily their limited spatial resolution could not meet the demands of clinicians or researchers. Optical imaging technology with the advantages of non-invasiveness, in situ detection, and real-time monitoring has been applied in clinics for fluorescence-guided surgery. However, the imaging depth is highly restricted by strong light scattering of tissues. Dual-model imaging has become the most attractive research method in recent years by integrating the advantages of each imaging modality to obtain accurate and reliable biological and structural information, thus contributing to the efficiency and accuracy of clinical diagnosis. The following are some representative findings of melanin/melanin-like nanoparticles applied in dual-model imaging-guided disease treatment.

3.2.1. PAI/MRI-guided therapy

Benefiting from non-invasiveness and versatile imaging methods, MRI owns excellent soft tissue contrast and unlimited penetration depth except for its poor sensitivity. Interestingly, PAI has high sensitivity and high resolution, while the limited penetration depth has puzzled many researchers. Therefore, PAI/MRI dual-modal imaging will possess excellent capacities, such as high resolution and deep tissue penetration in disease diagnosis and imaging-guided therapy. Inspired by the characteristic of melanin chelating with metal ions and inherent NIR absorbance, Sun et al. successfully prepared ultrasmall nanoparticles based on melanin-chelated Mn^{2+} ions (MNP-Mn) with a size of about 3.2 nm [149]. The ultrasmall melanin-based nanoparticle exhibited excellent PA activity and high relaxivity for MRI. Interestingly, they could be excreted quickly through renal and hepatobiliary pathways, showing better safety in vivo and great clinical translation potential for

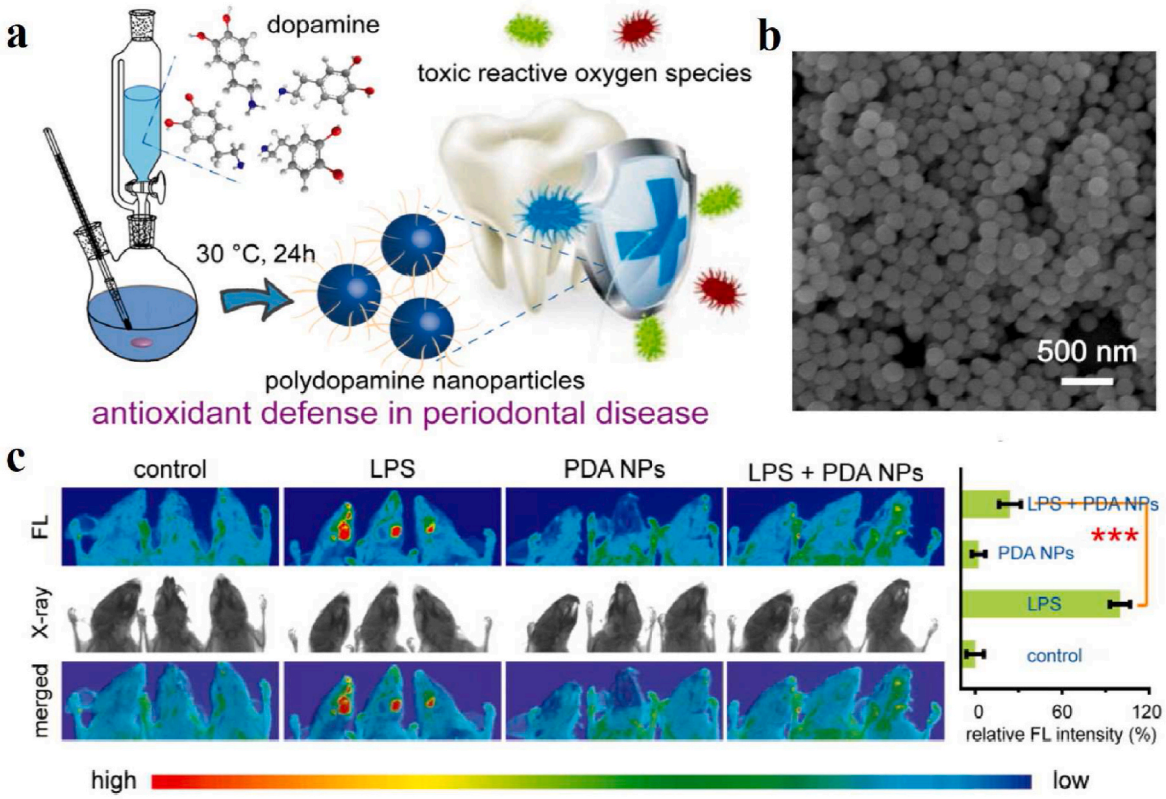

Fig. 8. (a) Schematic illustration of the synthesis of PDA NPs and their application to alleviate periodontal disease by scavenging toxic reactive oxygen radicals. (b) SEM image of synthesized PDA NPs. (c) *In vivo* fluorescence imaging was utilized to examine the ability of PDA NPs to scavenge ROS in terms of relative quantitative fluorescence intensity in normal mice and LPS-induced periodontal disease mice after 3 d of different treatments [144]. Copyright 2018, American Chemical Society.

cancer diagnosis and therapy. Moreover, they used gadolinium-based melanin nanoparticles as a dual-modal MRI/PAI contrast agent for the detection of orthotopic hepatocellular carcinoma imaging [160]. During MR and PA scanning, a significant signal difference can be found between the normal liver and the tumor region due to the different uptake abilities for nanoparticles, which are easier to identify the tumors from normal liver tissues for clinicians. To prolong the biological half-life and increase the passive accumulation, Zhang et al. successfully constructed bio-inspired melanin-based nanoliposomes (Lip-Mel) where melanin is encapsulated into PEGylated nanoliposomes for simultaneous PAI and

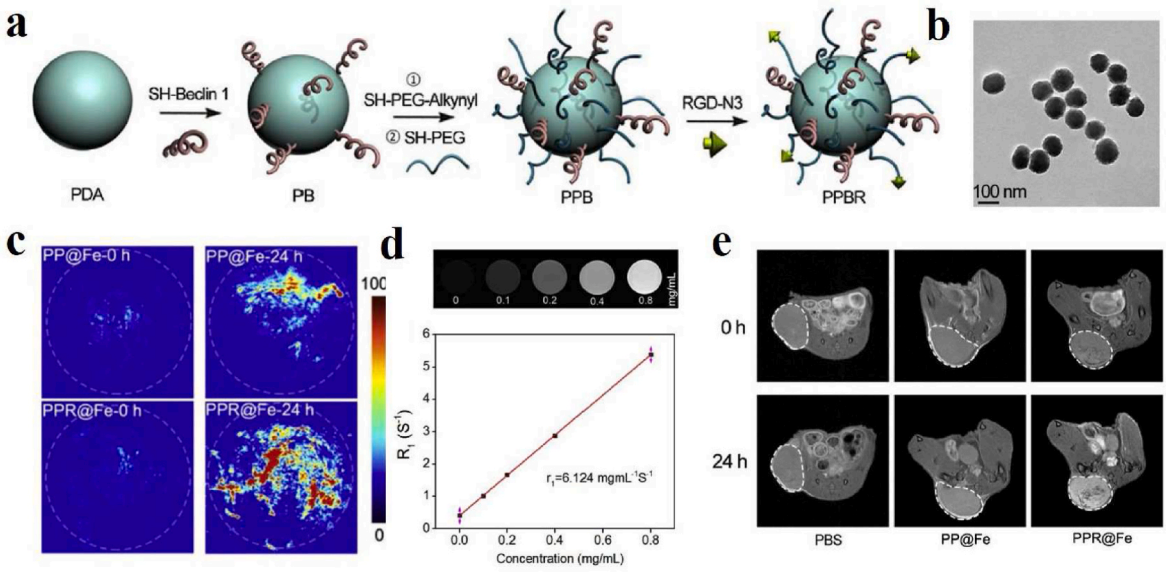

Fig. 9. (a) Schematic of the synthesis of PPBR nanoparticles. (b) TEM image of PPBR with the size of about 100 nm. (c) PA images of tumors before and 24 h after intravenous injection of PP@Fe and PPR@Fe. The white dashed circle represents the tumor region. (d) MRI images of different concentrations of PP@Fe in deionized water, relaxation rate R1 as a function of the concentration of iron ions in PP@Fe. The relaxation value r_1 is derived from the slope of the curve. (e) T1WI images of tumors before and 24 h after intravenous injection of PBS, PP@Fe, and PPR@Fe. White dashed circle outlines the tumor sites [151]. Copyright 2019, Elsevier.

T1WI with high biocompatibility, providing the potential for therapeutic guidance and monitoring [150]. To effectively inhibit tumor growth, Zhou et al. fabricated a dual peptide RGD- and beclin 1-modified and PEGylated melanin-like PDA nanoparticles (PPBR) for tumor-targeted and autophagy induction-associated photothermal cancer therapy (Fig. 9) [151]. TEM image of PPBR showed that the average size approximately was 101.96 nm with a spherical shape (Fig. 9b). At the same time, the PP@Fe and PPR@Fe were synthesized for evaluating the in vivo biodistribution of the nanoparticles through PA imaging and MR imaging. The T1-weighted signal of PP@Fe *in vitro* increased linearly with concentration (Fig. 9d). As shown in Fig. 9c and e, in vivo PA imaging and MR imaging showed that the tumor signal of mice injected with PPR@Fe intravenously was significantly higher than that of PP@Fe, which suggested that RGD could enhance the accumulation of the nanoparticles in the tumor. Besides, the animal experiments revealed that PPBR could effectively inhibit tumor growth in breast tumor models through RGD-mediated tumor targeting and beclin-1-modified autophagy up-regulation. Meanwhile, Feng et al. developed melanin-coated magnetic nanoparticles loading the Wnt signaling inhibitor obatoclax (OBX-MMNs) for MRI/PAI guided mild hyperthermia-enhanced chemotherapy [152]. Besides, Chen's team prepared a nanoagent based on MNPs-coupled NIR dye IR820 (IR820-PEG-MNPs), achieving enhanced PA performance and PTT effect, which could selectively ablate in-situ liver tumors under PA/MR imaging guidance [153].

Other researchers reported an angiopep-2 functionalized and manganese-doped eumelanin-like nanocomposites loading the neuroprotective agent curcumin (ANG-MnEMNPs-Cur, AMEC) as a

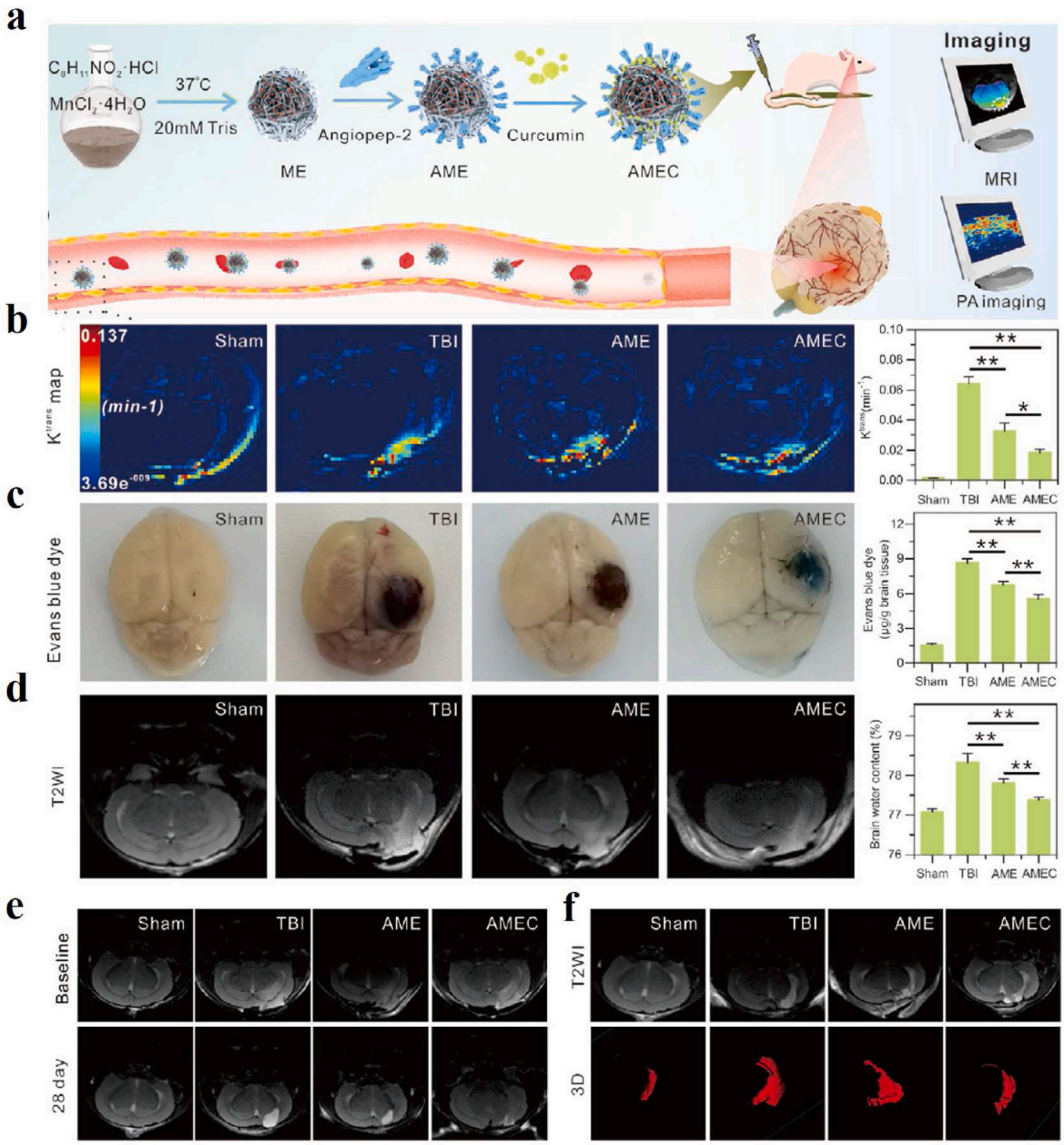

Fig. 10. (a) Schematic of the synthesis process of AMEC with T1-T2 MR and PA imaging capabilities and its use as a potential tool for TBI treatment. (b) Representative Ktrans map derived from DCE-MR imaging and quantitative analysis of the brain one day after treatment. (c) Representative EB-staining images and quantitative analysis in the brain one day after treatment. (d) Representative T2WI MR images and quantitative analysis of brain edema one day after treatment. (e) Representative T2WI images of the lesion volumes before and 28 days after treatment. (f) Representative T2WI images of ventricular volumes before and 28 days post-treatment [154]. Copyright 2022, Wiley-VCH.

theranostic tool, which was observed to be efficient accumulation in lesions of traumatic brain injury (TBI) mice models by T1–T2 MR and PA dual-modal imaging (Fig. 10) [154]. Dynamic contrast-enhanced (DCE)-MR imaging, Evans blue (EB) staining, and T2WI MR image results demonstrated that AMEC could protect the blood-brain barrier efficiently (Fig. 10b–d). The T2WI of lesion volumes and T1WI of ventricular volumes results indicated that reparation of the brain tissue after AMEC treatment could reduce the development of hydrocephalus with better efficiency (Fig. 10 e-f).

3.2.2. PAI/PET-guided therapy

In order to achieve personalized treatment, as the only imaging strategy that can trace the metabolism of theranostic agents, PET is usually used to provide detailed information about the distribution of nano-agents in the human body. However, PET is not convenient for imaging tissues due to the limitation of low image resolution. Combined with rich optical contrast and high ultrasonic spatial resolution, PAI is often applied to collect the distribution information of drug-loaded systems and for real-time imaging-guided therapy. Combining PET with PA imaging could track the activity of theranostic platforms in vivo with high temporal resolution. Zhang et al. constructed melanin–drug system using ultrasmall melanin nanoparticles (MNPs) and hydrophobic sorafenib (SRF) [28], which possess high drug-loading capacity because of the high surface-to-volume of ultrasmall MNPs (Fig. 11a and b). Interestingly, the PEG-MNPs bind to SRF by intermolecular forces to form larger NPs with a size of about 60.0 nm (Fig. 11c). Through

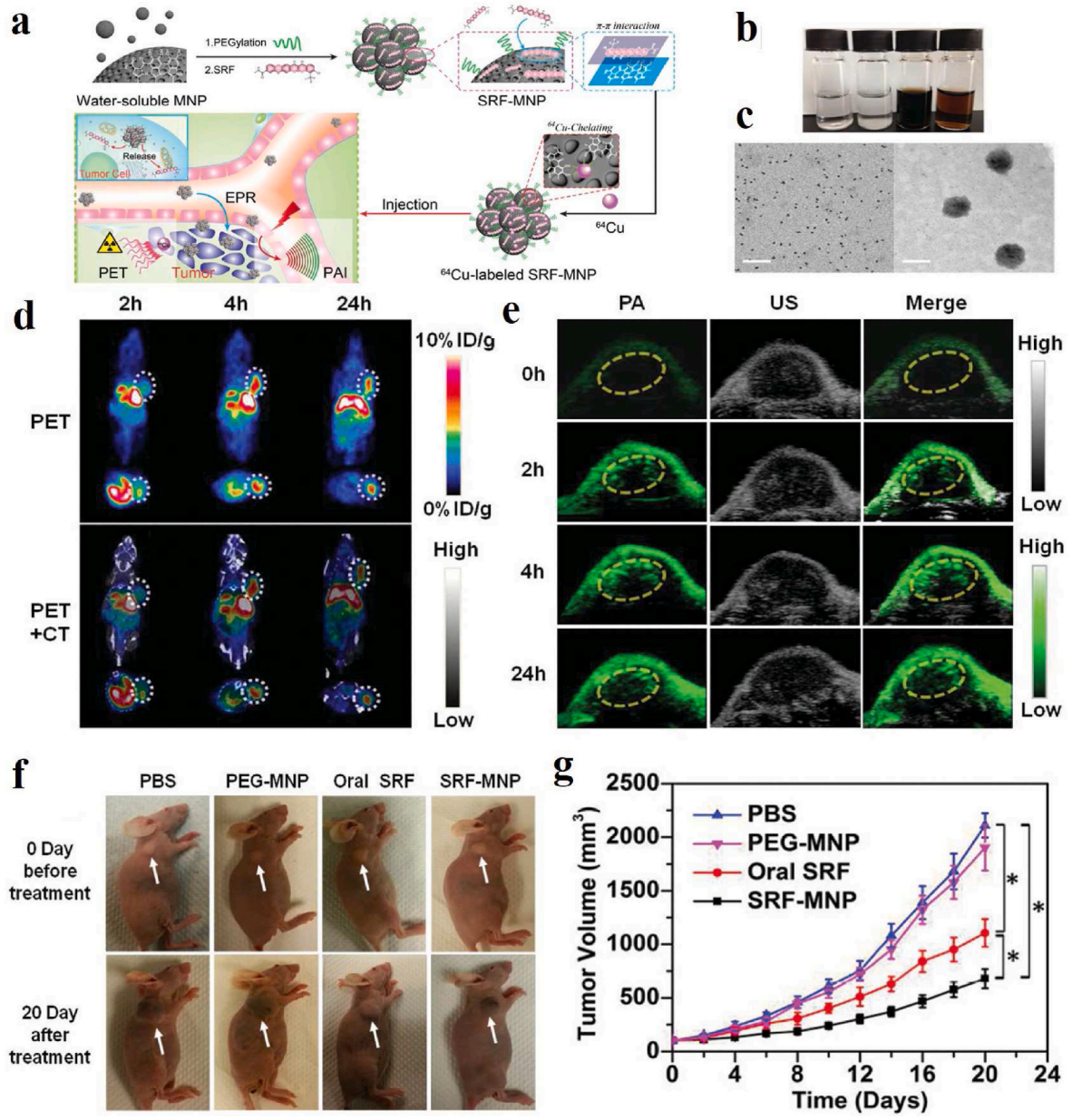

Fig. 11. (a) Schematic illustration of the preparation of ^{64}Cu-labeled SRF-MNP nanoparticles and PET and PAI dual-modal imaging-guided therapy of HepG2 tumor in vivo. (b) photographs of PBS, SRF precipitated in PBS, PEG-MNP dispersed in PBS, and SRF-MNP dispersed in PBS. (c) TEM images of PEG-MNP (left) and SRF-MNP (right), scale bar = 50 nm. (d) PET and PET/CT images after tail vein injection of ^{64}Cu-labled SRF-MNP nanoparticles at 2 h, 4 h and 24 h. White dotted line outlines the tumor sites. (e) PA images of tumor-bearing mice before and after tail vein injection of SRF-MNP nanoparticles at 2 h, 4 h and 24 h. Yellow dotted line envelops the tumor region. (f) Representative photographs of HepG2 tumor mice after 20 days of different treatments. (g) Tumor growth curves of HepG2 tumor mice after 20 days of different treatments [28]. Copyright 2015, Wiley-VCH. (For interpretation of the references to color in this figure legend, the reader is referred to the Web version of this article.)

chelating SRF-MNPs with $^{64}Cu^{2+}$, the biodistribution of SRF-MNPs in vivo and the highest uptake in the tumor were revealed by PET/CT and PA imaging (Fig. 11d and e), both of which displayed the consistent trend of change in the tumor, suggesting the successful penetration of SRF-MNPs in tumor site. Furthermore, the volume of tumors treated with SRF-MNPs was the smallest, as shown in Fig. 11f–g, which proved the excellent anti-tumor effect of SRF-MNPs.

3.2.3. PAI/FLI-guided therapy

PAI combines the high contrast of optical imaging with the high resolution of ultrasound imaging. Combining PAI and FLI, dual-mode imaging demonstrates high resolution and sensitivity in disease diagnosis and imaging-guided therapy. In our previous work, human umbilical vein stem cells were rapidly labeled with NIR-II fluorescent dye-modified melanin nanoparticles (MNP-PEG-H2), which enabled long-term tracking of human umbilical artery stem cells (hUMSCs) by NIR-II FL/PA bimodal imaging and showed human umbilical vascular stem cell-based liver regeneration in acute liver failure [155]. In oncology treatment, the combination of NIR fluorescent dye not only endows melanin nanoparticles FLI property, but enhances the overall performance of PAI and PTT [161,162], which can precisely delineate tumors, monitor the real-time accumulation of therapeutic agents, and obtain optimal treatment results. Sun et al. designed a multifunctional drug delivery platform combining discrete Pt(II) metal rings and a NIR-II fluorescent dye into melanin dots, which can be utilized for NIR-II FL/PA dual-modal imaging-guided chemo-photothermal synergistic therapy

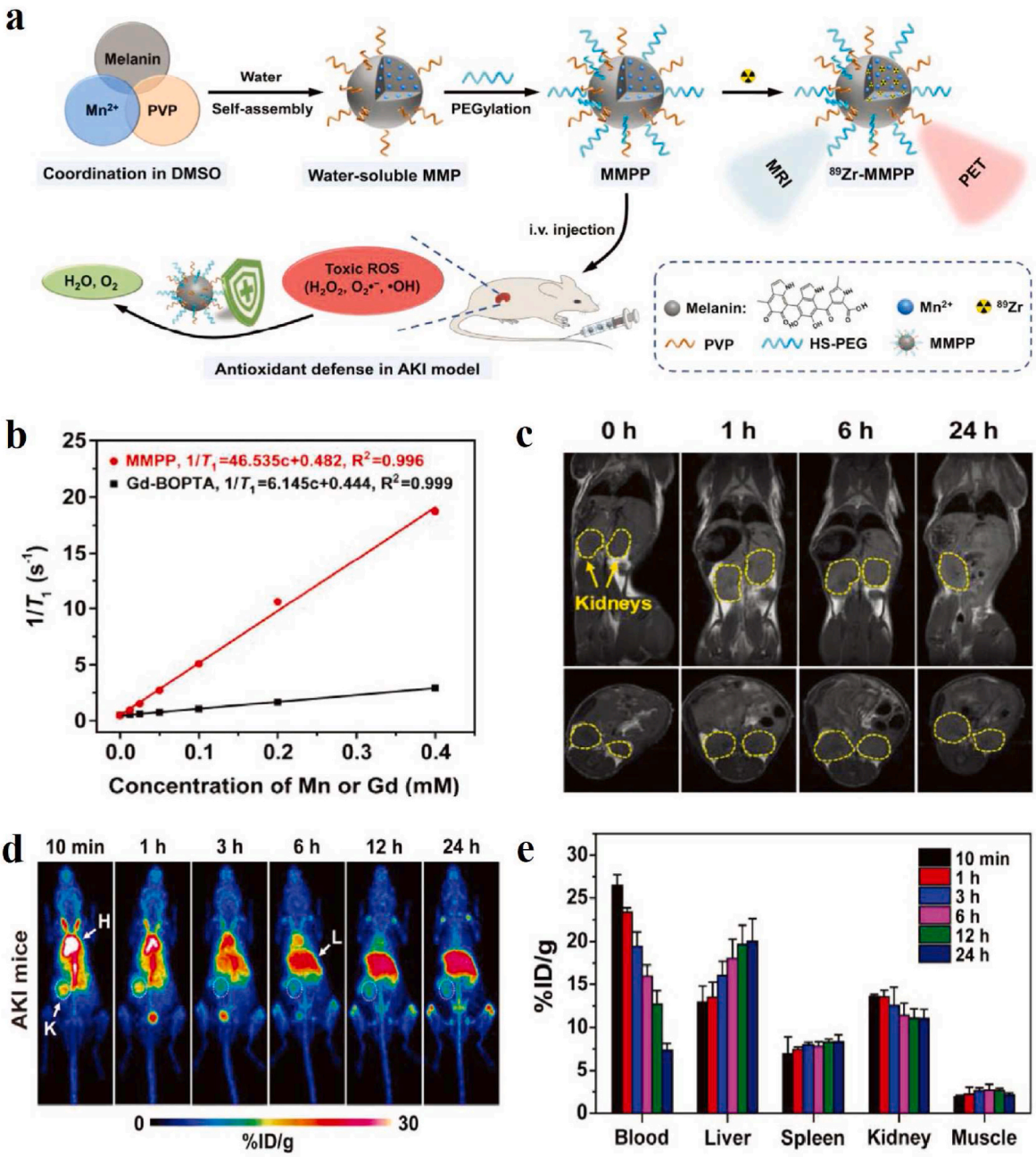

Fig. 12. (a) MMPP nanoparticle preparation and its application in PET/MR dual-modality imaging-guide antioxidant treatment of AKI. (b) T1 relaxation rate curves at 4.7 T of different concentrations of MMPP and Gd-BOPTA. (c) Coronal and axial MRI images of MMPP nanoparticles in AKI mice before and after injection at different time points. Kidneys are circled in yellow dashed lines. (d) PET images of AKI mice injected with ^{89}Zr-MMPP at different time points. (e) Distribution of ^{89}Zr-MMPP uptake in blood, liver, spleen, kidney and muscle of AKI mice at different time points after injection [158]. Copyright 2019, Wiley-VCH. (For interpretation of the references to color in this figure legend, the reader is referred to the Web version of this article.)

[156]. The nanoplatform has good solubility, biocompatibility, and in vivo stability. PAI and in vivo NIR-II FLI confirmed its effective accumulation at the tumor site with a good signal background ratio and well distribution.

3.2.4. MRI/FLI-guided therapy

FLI is favorable for visualizing the real-time dynamics in living organisms, benefiting from minimal tissue absorption, scattering, and autofluorescence in the NIR-I/II window, and inheriting the quick feedback property of optical imaging. However, the depth of tissue penetration is low [163]. As we all know, MRI is one of the most important clinical tools, which can visualize internal anatomical structures with high spatial resolution and deep tissue penetration, but poor sensitivity restricts further optimization and application [164]. Moreover, both imaging modalities are non-invasive and non-radioactive. Therefore, the combination of FLI and MRI is expected to provide a powerful imaging modality for more accurate biomedical treatment. In 2017, Cho et al. developed silica-coated Gd-chelated melanin nanoparticles (Gd-Mel@SiO_2 NPs) for MRI/FLI-guided cancer therapeutic [157]. By chelating with Gd^{3+}, MRI contrast property of the Gd-Mel@SiO_2 NPs was significantly improved. Moreover, after labeled with fluorescent molecules TRITC, enhanced fluorescent intensity was achieved by the silica coating that prevented the innate fluorescent deactivation property of melanin. These nanoparticles allowed in vivo dual-modal contrast-enhanced MR and fluorescent imaging and image-guided catheter-directed infusion for photo-heating cancer therapy.

3.2.5. MRI/PET-guided therapy

As one strong biological molecular imaging and clinical diagnosis tool, MRI could help us obtain abundant soft issue anatomical lesions without ionizing radiation. PET shows ultrahigh sensitivity and tissue penetration, which could accurately display biomolecular metabolism in vivo and conduct quantitative analysis. Concerning multimodal imaging systems, MRI combined with PET would produce a significant effect of one plus one greater than two. Even this perfect combination model has been translated into clinical medicine named PET-MR. Cai and Huang's group designed an ultrasmall PEGylated Mn^{2+}-chelated melanin nanoparticle (MMMP) as a natural antioxidant defense nanoplatform for the treatment of glycerol-induced AKI (Fig. 12a) [158]. By assembled T1-weighted MR and PET imaging modalities, the ^{89}Zr radiolabeling of MMPP nanoparticles allows visualization of AKI treatment assessment. The T1 relaxivity was shown in Fig. 12b. We could find that the T1 relaxation rate (r1) of MMPP nanoparticles was ≈7.5-fold higher than that commercial contrast agent of gadobenate dimeglumine. After intravenous injection of MMPP nanoparticles, the kidneys in AKI mice present the increased T1-weighted MR signals (Fig. 12c). PET imaging also demonstrated that the accumulation of ^{89}Zr-MMPP nanoparticles in the kidneys of AKI mice gradually began to enhance (Fig. 12d), which was roughly consistent with MR imaging. Fig. 12e demonstrated the uptake of ^{89}Zr-MMPP nanoparticles in various tissues of AKI mice at different time points, and it could be seen that in addition to the liver, the kidneys also have high uptake and retention, which is conducive to the scavenging of toxic ROS by melanin nanoparticles to alleviate AKI.

3.2.6. FLI/PET-guided therapy

Although NIR-II fluorescence imaging has shown great potential for tumor image-guided resection due to its real-time imaging and high resolution, its limited depth of penetration and lack of quantification still limit its further application. In contrast, PET is not limited by tissue penetration depth, has high sensitivity and accurate quantification, however, it has low spatial resolution, is time-consuming, and is difficult to apply for intraoperative guidance. Therefore, combining NIR-II FLI with PET dual-modality imaging can overcome these drawbacks and has important significance for clinical tumor diagnosis and treatment because of complementary advantages. Zhang et al. integrated three kinds bioinspired nanomaterials (melanin dot, mesoporous silica nanoparticle, and supported lipid bilayer), NIR-II dye CH-4T, and PET radionuclide ^{64}Cu into a hybrid NIR-II FLI/PET nanoplatform (CH-4T/SLB-MSN-Mdot/$^{64}Cu^{2+}$) for dual-modality imaging-guided surgical resection of tumor (Fig. 13). The nanoplatform demonstrated high sensitivity and excellent penetration depth in PET imaging of A431 tumors in mice. Interestingly, the incorporation of CH-4T into nanoparticles resulted in a 4.27-fold fluorescence enhancement, helping identify the vasculature and delineate the tumor during surgery accurately. In a word, the hybrid bimodal nanoprobe has a broad prospect in tumor detection and accurate resection during surgery [159].

3.3. Tri-modal imaging-guided therapy

In recent years, tri-modal imaging-guided therapy has gradually become a research hotspot. Benefiting from the inherent chelation properties of metal ions, wide optical absorption, and accessible modification, water-soluble melanin/melanin-like nanoparticles could be a promising candidate for tri-model imaging. Fan et al. developed a multifunctional biopolymer nanoplatform based on cyclic c(RGDfC) peptide conjugated ultrasmall (<10 nm) water-soluble melanin nanoparticles (MNPs), which can serve not only as a PA contrast agent but also as a nanoplatform for PET and MRI [35]. By embedding these ultrasmall MNPs into the cavity of apoferritin (APF), the constructed multimodal imaging nanoplatform exhibited good tumor uptake, high specificity, and high tumor contrast, in which APF played synergistic roles of guaranteeing targeting and stability of the nanoplatform [165]. Besides, bio-inspired melanin nanoparticles doped simultaneously with Fe^{3+}, Bi^{3+}, and iodine were tested for improving the performance of triple imaging by MRI, CT, and SPECT [166]. Other metal ions-chelated melanin nanoparticles are constantly being constructed for multimodal imaging [167]. In addition to the development and application of tri-modal imaging, we could believe that multifunctional nano-theranostics based on melanin/melanin-like nanoparticles lead to important practical significance. The following are some representative findings of melanin/melanin-like nanoparticles applied in tri-model imaging-guided disease therapy.

Integration of MRI, PET, PAI, CT, or FLI modalities is a prerequisite for accurate diagnosis of tumors to provide complementary information and imaging-guided therapy. The multiple properties inspire the melanin/melanin-like nanoparticles to possess great potential in multimodal imaging-guided therapy. Lin et al. designed ^{64}Cu-labeled magnetic melanin nanoparticles (^{64}Cu-MMNs) [168], of which ^{64}Cu was strongly bonded for PET imaging. The presence of super-paramagnetic Fe_3O_4 made an enhanced MRI signal. The melanin possessed strong NIR absorbance and was prepared as a coating layer for PAI and photothermal therapy. More interestingly, MMNs can effectively resist both ultraviolet and γ irradiation. In particular, the combination of MRI, PET, and PAI could compensate for the limitations of each other, thus resulting in significantly enhanced efficiency compared to their individual imaging. Capitalizing on these facts, Hong et al. prepared Gd^{3+} and $^{64}Cu^{2+}$ loading melanin dots (Gd-*M*-dots) for MRI, PET and PAI, meanwhile providing a versatile nanoplatform for biomedical imaging applications [167]. In addition, Wang et al. developed a radionuclide-^{64}Cu-labeled doxorubicin-loaded PDA-gadolinium-metallofullerene core-satellite nanotheranostic agent [169], which not only overcomes low relaxivity and high risk of released-Gd-ions-associated toxicity of clinical MR contrast agent but could be performed PAI and PET multimodal imaging-guided chemo-photothermal cancer therapy. Although melanin or melanin-like nanoparticles have vast perspectives in multimodal imaging to enhance the sensitivity and specificity of the theranostics process, the weak NIR absorption makes them a poor PTT effect for tumor therapy. Recently, our group presented a multifunctional theranostic nanoplatform based on melanin-coated gold nanorods (GNR@MNP-Gd-^{64}Cu) that exhibits excellent PAI/MRI/PET multimodal imaging ability and photothermal effects [170]. The melanin

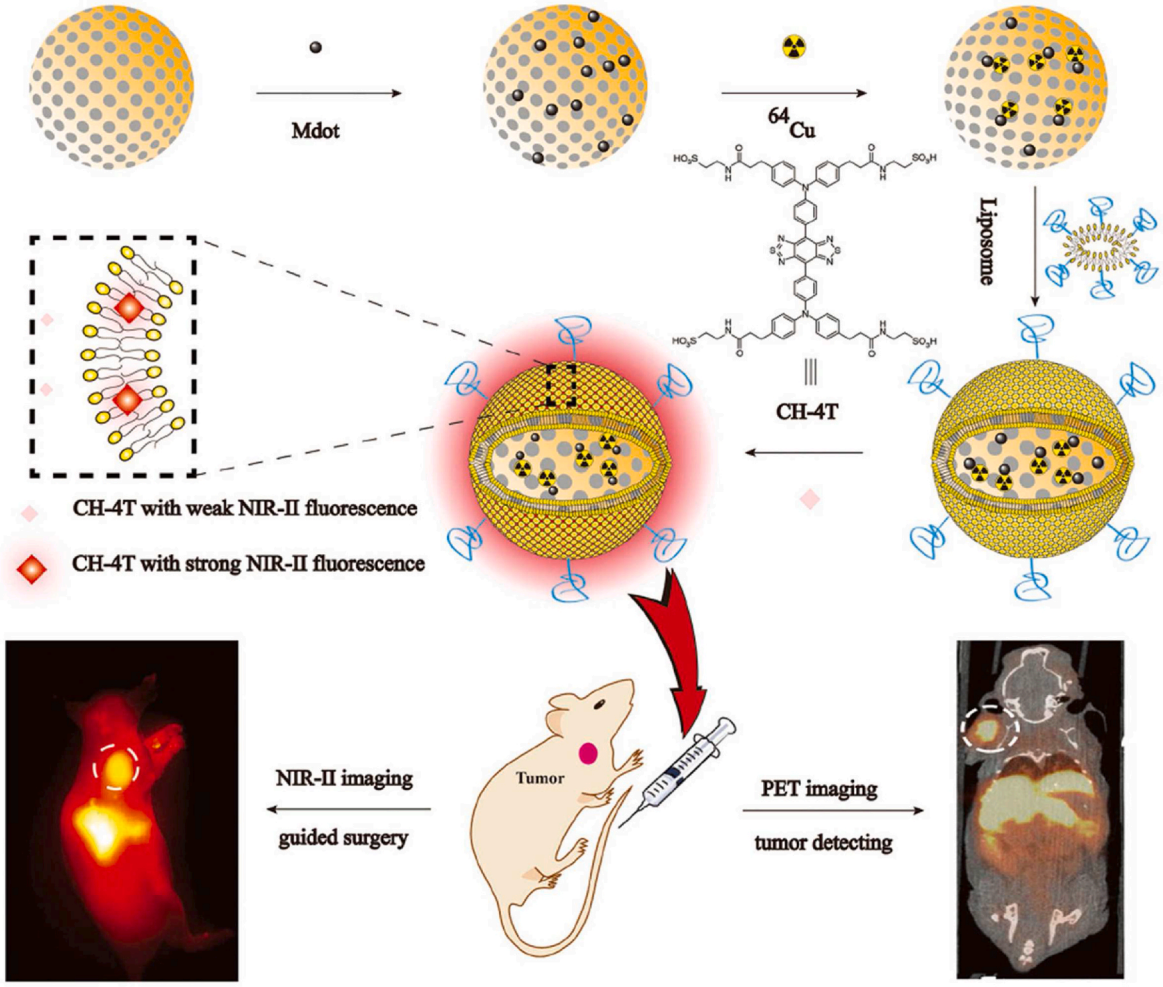

Fig. 13. CH-4T/SLB-MSN-Mdot/$^{64}Cu^{2+}$ nanoprobe construction and its tumor detection by PET imaging and NIR-II fluorescence imaging-guided surgery [159]. Copyright 2019, Wiley-VCH.

nanoparticles significantly inhibit the cytotoxicity of the cetyltrimethylammonium bromide bilayer template on the surface of GNR and confer excellent PET/MR imaging properties to GNR. In addition, the introduction of GNR into melanin nanoparticles also greatly improves the NIR absorption performance, leading to excellent PA imaging and tumor PTT. Besides, Chen et al. synthesized melanin nanoparticles (Au-M) with a diameter of about 120 nm and modified tunable small gold nanoparticles on their surface. The Au-M nanocomposites have strong X-ray attenuation coefficients and good biocompatibility. After injection of Au-M in mice, the tumors could be detected by X-ray CT, PA, and thermal imaging, leading to thermal ablation of the tumors at the same time [171]. He et al. developed a magnetic/RGD dual-targeting multifunctional nanotheranostic agent (denoted as RMDI) based on melanin-coated magnetic nanoparticles (MMNs), coloaded with DOX and ICG for FL/MR/PA tri-modal imaging-mediated synergetic photothermal-enhanced chemotherapy of U87MG tumor [172].

The development of activatable multimodal imaging-guided nanoplatforms to simultaneously improve diagnostic and therapeutic performances while reducing side effects is highly attractive for precision cancer medicine. Given the skin damage and health problems caused by phototoxicity during PDT, Dong et al. synthesized a multifunctional composite based on dopamine and calcium carbonate hollow nanoparticles ($CaCO_3$-PDA) and utilized them as a photosensitizer chlorin e6 (Ce6)-loading nanoplatforms for imaging-guided cancer PDT with efficient skin photoprotection (Fig. 14) [173]. The morphology and structure of $CaCO_3$-PDA nanoparticles can be precisely adjusted by changing the feeding ratio of dopamine and calcium chloride ($CaCl_2$). As described in Fig. 14b, when the mass feeding ratio of dopamine and $CaCl_2$ was 2:150, the $CaCO_3$-PDA nanoparticles showed a uniform and well-defined hollow structure, and the TEM results showed that the average diameter was 168 nm, and the thickness of the shell was 44 nm (Fig. 14c). Furthermore, elemental mapping analysis strongly proved the existence and content of N, O, and Ca in the $CaCO_3$-PDA nanoparticles (Fig. 14d–e). Because of native optical absorbance and intrinsic binding with metal ions Mn^{2+}, the nanoparticles could perform PAI and MRI in vivo (Fig. 14f–g). Under neutral pH, the photoactivity of Ce6 is quenched by the strong absorption of PDA, whereas in the tumor microenvironment with low pH, Ce6 can be activated, fluorescence is restored, and single-linear oxygen generation is enhanced. After the intravenous administration of Ce6@$CaCO_3$-PDA-PEG, FLI showed efficient tumor accumulation (Fig. 14h). The blood circulation of Ce6@$CaCO_3$-PDA-PEG with a long blood half-life ($t1/2(\alpha) = 1.39 \pm 0.05$ h, $t1/2(\beta) = 16.41 \pm 2.26$ h), was displayed in Fig. 14i. The biodistribution in Fig. 14j showed that the tumor accumulation of Ce6@$CaCO_3$-PDA-PEG in mice reached a peak of ~10.0 % ID/g after intravenous administration at 24 h. This work provided a method for multimodal imaging combined with high anti-tumor PDT efficacy and further reduced skin phototoxicity.

Recently, Zhu's group fabricated a novel biocompatible melanin nanoprobe (PMNs–II–813) coupled with a highly specific prostate-specific membrane antigen small molecule inhibitor for PET/MRI/PAI multimodal imaging guided radioisotope combined photothermal

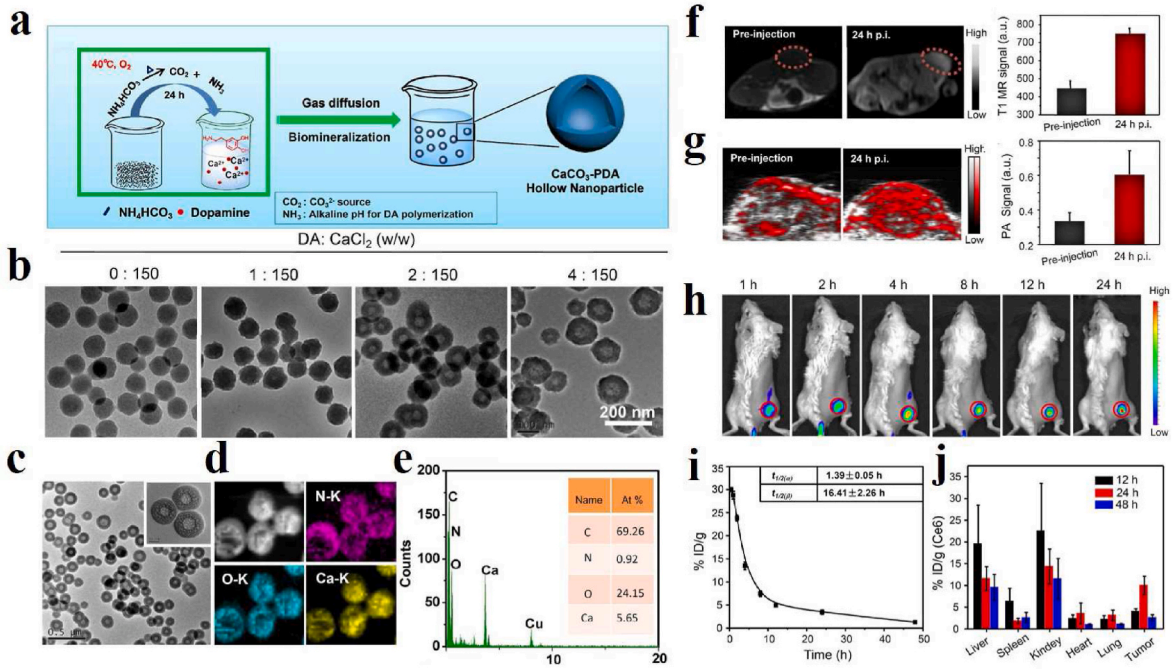

Fig. 14. (a) Preparation of $CaCO_3$-PDA-PEG hollow nanoparticles. (b) TEM images of nanoparticles prepared with different feed ratios of dopamine and $CaCl_2$. (c) TEM image of $CaCO_3$-PDA hollow nanoparticles prepared with 2:150 feed ratio of dopamine and $CaCl_2$. (d) EDS image of $CaCO_3$-PDA hollow nanoparticles showing distribution of N, O and Ca. (e) EDX spectra of $CaCO_3$-PDA hollow nanoparticles. (f) T1WI MR images of 4T1 tumor before and 24 h after $CaCO_3$-PDA(Mn)-PEG injection and intensity analysis of tumor site. (g) PA images of 4T1 tumors before and 24 h after $CaCO_3$-PDA-PEG injection and intensity analysis of tumor areas. (h) *In vivo* fluorescence imaging of 4T1 tumor-bearing mice injected intravenously with Ce6@$CaCO_3$-PDA-PEG. (i) Circulatory half-life after intravenous injection of Ce6@$CaCO_3$-PDA-PEG. (j) Biodistribution of Ce6@$CaCO_3$-PDA-PEG in 4T1 tumor-bearing mice at different time intervals (12, 24, and 48 h) after intravenous injection of Ce6@$CaCO_3$-PDA-PEG [173]. Copyright 2018, American Chemical Society.

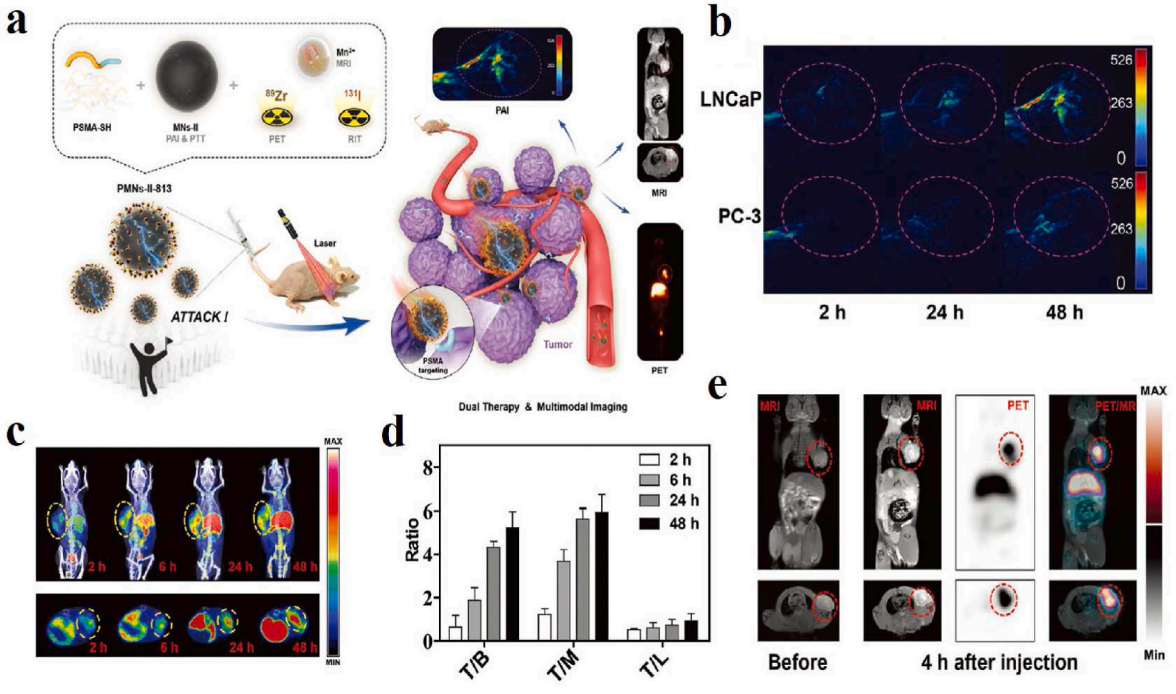

Fig. 15. (a) Schematic illustration of PMNs–II–813 nanoprobe for PET/MRI/PAI tri-modal imaging-guided RIT and PTT of prostate cancer. (b) PA images of LNCaP and PC-3 tumor after tail vein injection of Mn-PMNs-II for 2 h, 24 h, and 48 h. (c) Small animal PET/CT images of LNCaP tumors in coronal and axial positions obtained 2 h, 6 h, 24 h, and 48 h after tail vein injection of PMNs–II–813. (d) The radioactivity distribution of PET/CT images was assessed by the T/B, T/M, and T/L ratios. (e) PET/MRI images of LNCaP tumors before and after tail vein injection of PMNs–II–813 at 4 h [174]. Copyright 2021, Wiley-VCH.

therapy (Fig. 15a) [174]. After intravenous injection of PMNs–II–813, the PA signal in the tumor site was significantly improved after 48 h compared with after the first 2 h (Fig. 15b). Representative PET images in Fig. 15c showed the highest tumor accumulation at 48 h post-injection, where tumor-to blood (T/B), tumor-to-muscle (T/M), and tumor-to liver (T/L) ratios were 5.23 ± 0.72, 5.93 ± 0.82, and 0.93 ± 0.33, respectively (Fig. 15d), demonstrating the radioactivity was mainly concentrated in the heart, liver, spleen, intestine, and tumor. In dual PET/MRI imaging (Fig. 15e), there was an enhanced MR signal with PMNs–II–813LNCaP in tumor-bearing mice at 4 h after drug injection. At the same time, PET also showed high PMNs–II–813 uptake at the tumor site and the liver. Moreover, PET/MRI using PMNs–II–813 allowed real-time monitoring of the treatment effect for more than a week, demonstrating the ability of multimodal treatment of prostate cancer. ^{131}I labeling also equipped the nanoprobes with the ability to perform radioisotope therapy (RIT). The combination of PTT and RIT had a significant inhibitory effect on the prostate cancer.

4. Conclusions and future perspectives

Melanin, as one kind of ubiquitous biological pigment, is widely distributed in living organisms, and is generated by oxidation and polymerization of self-assembling building blocks, such as tyrosine, L-DOPA, and dopamine. In this review, natural melanin nanoparticles extracted from bacteria, fungus, black sesame seeds, human hair, and ink sac of cuttlefish have been reported in detail. The various preparation strategies of synthetic melanin-like nanoparticles have been described to improve their physical and chemical properties (size, light absorption, antioxidant, etc.). In recent years, natural melanin/melanin-like nanoparticles have aroused extensive research interest owing to their excellent biocompatibility and biodegradability, inherent NIR-absorbance, radioprotection, antioxidant activity, free-radical scavenging, metal ion chelation, drug loading, and functionalized modifications. Inspired by the fascinating properties and versatile functionality of melanin/melanin-like nanoparticles, the design and construction of novel multifunctional nanoplatforms for imaging-guided disease therapy could be achieved on one nanoplatform to maximize the theranostic performance, which from single-modal imaging to multimodal imaging, integrating molecular imaging (PAI, MRI, PET, FLI, and CT) with the treatment of various diseases (surgical therapy, chemotherapy, radiotherapy, PTT, PDT, immunotherapy, gene therapy, iron overload, antioxidant therapy, and so on), realizing visual drug delivery and treatment of tumor, osteoarthritis, acute kidney injury, acute liver injury, acute peritonitis and acute lung injury, periodontitis, traumatic brain injury, etc. Additionally, surface modification or combination with functional molecules and targeting ligands such as hyaluronic acid, peptides, or antibodies is helpful to prolong circulation time in the body, step over various biological barriers, and increase accumulation in the lesion site, which can further enhance the diagnostic accuracy and therapeutic efficiency. Despite tremendous efforts and considerable progress in melanin/melanin-like nanoparticles as a robust and versatile nanoplatform have been achieved, there are still a number of issues that need to be addressed before eventual clinical translation.

For scientific challenges and technical issues: (1) To meet clinical translation and commercial needs, more facile, low-cost, and large-scale fabrication procedures need to be exploited, and their repeatability needs to be validated. For natural melanin nanoparticles, standardized extraction, purification procedures, and corresponding quality control standards should be established to obtain uniform characteristics. While for melanin-like nanoparticles, more efforts should be devoted to understanding the detailed polymerization mechanisms, defined chemical structures, and structure-property-function relationships. Moreover, strict quality control such as precise control of reaction conditions should be carried out to obtain consistency and stability of different batches of products. (2) The biosecurity of melanin-based nanomaterials should be systematically evaluated before their clinical translation. Immunogenicity and other side effects of residual components (proteins and biomolecules) in natural melanin extracted from various organisms should be systematically investigated. Although melanin-like nanoparticles are productive and biocompatible, the metabolism, biodegradation, and potential implication on organisms from long-term administration are still unclear, which require further explorations systematically and thoroughly. (3) Given the relatively weak NIR absorbance compared with traditional metal-based nanoparticles, the PA signals of melanin/melanin-like nanoparticles are insufficient to meet the clinical requirements. Therefore, advanced tailored strategies should be required for better theranostic applications. (4) Melanin-based multifunctional nanoparticles can integrate the diagnosis, treatment, monitoring, and prognosis of diseases into a single nanoplatform. Thus, more advanced instruments with multiple excitation sources and deeper tissue penetration are ideal for synchronous multimodal images and multiple synergistic therapies. However, nanodrugs should be designed according to the characteristics of the lesion instead of blindly pursuing multifunctions, to guarantee their physiological stability, repeatability, imaging accuracy, and therapeutic effect. (5) In disease treatment, regarding heterogeneity, unique microenvironment, and easily metastasized characteristics in the tumor, immunotherapy-based synergistic therapy may be a fascinating option, especially for PTT-immunotherapy, which could be readily implemented in a simple system to activate the immune system and eliminate distant metastatic tumor cells. Another direction is the exploration of melanin/melanin nanoparticles as a theranostic platform and expanding their application for the treatment of more types of diseases. In addition, melanin-based nanotherapeutics prefer to be synthesized directly in situ, without the introduction of exogenous materials, and to treat the disease only through endogenous biocatalytic reactions triggered by the microenvironment of the lesion, which would provide better specificity and biosafety.

Prospects for clinical application: Natural melanin nanoparticles and melanin-like nanoparticles all exhibit fascinating physicochemical characteristics, which make them highly intriguing for for image-guided precise therapy for various diseases. Natural melanin nanoparticles contain a variety of amino acids and polysaccharides, etc., which may have better biocompatibility, while melanin-like nanoparticles can be adjusted in size, morphology, microstructure and function by controlling the preparation process, so as to realize the precise treatment of the disease. Therefore, researchers can select the right melanin nanoparticles for their needs, such as the progression of the disease (matching the appropriate imaging modality) and the additional functions they want to achieve (PTT, antioxidant therapy, etc.), and then integrate the diagnosis, treatment, monitoring, and prognosis of the disease into a single nano-based platform to maximize the functionality of melanin and melanin-like nanoparticles. Meanwhile, the construction of biodegradable and renal metabolizable melanin nanoparticles (either naturally derived or synthetic) with appropriate size and function has better prospects for clinical applications.

In conclusion, this review systematically, comprehensively, and in detail describes past recent advances in imaging-guided therapy with melanin/melanin-like nanoparticles, which is expected to deepen our understanding of melanin and its derived nanomaterials in biomedical applications and to facilitate further clinical translation of melanin-based nanotheranostic agents.

CRediT authorship contribution statement

Jinghua Sun: Conceptualization, Data curation, Writing - original draft. **Yahong Han:** Conceptualization, Writing - original draft. **Jie Dong:** Data curation, Writing - original draft. **Shuxin Lv:** Data curation, Writing - original draft. **Ruiping Zhang:** Conceptualization, Writing - review & editing.

Declaration of competing interest

We declare that we do not have any commercial or associative interest that represents a conflict of interest in connection with the work submitted.

Data availability

Data will be made available on request.

Acknowledgements

This work has been financially supported by the National Natural Science Foundation of China (No. 32271429, 82120108016, 82071987), China Postdoctoral Science Foundation (No. 2022M722002). Natural Science Research Project of Shanxi Province (No. 202203021211243). National Ten Thousand Talents Program (SQ2022RA2A300118), Research Project Supported by Shanxi Scholarship Council of China (No. 2020-177), Fund Program for the Scientific Activities of Selected Returned Overseas Professionals in Shanxi Province (No. 20200006), Four Batches of Scientific Research Projects of Shanxi Provincial Health Commission (No. 2020TD11, NO: 2020SYS15, 2020XM10). Key Laboratory of Nano-imaging and Drug-loaded Preparation of Shanxi Province (No. 202104010910010).

References

[1] Q. Chen, et al., Recent advances in different modal imaging-guided photothermal therapy, Biomaterials 106 (2016) 144–166.
[2] M. Chetrit, et al., Imaging-guided therapies for pericardial diseases, JACC Cardiovasc Imaging 13 (6) (2020) 1422–1437.
[3] B. Xie, et al., Supramolecular biomaterials for bio-imaging and imaging-guided therapy, Eur. J. Nucl. Med. Mol. Imag. 49 (4) (2022) 1200–1210.
[4] E.K. Lim, et al., Nanomaterials for theranostics: recent advances and future challenges, Chem Rev 115 (1) (2015) 327–394.
[5] G. Chen, et al., Nanochemistry and nanomedicine for nanoparticle-based diagnostics and therapy, Chem Rev 116 (5) (2016) 2826–2885.
[6] Y. Tao, et al., Metal nanoclusters: novel probes for diagnostic and therapeutic applications, Chem. Soc. Rev. 44 (23) (2015) 8636–8663.
[7] W. Chen, et al., Structural-engineering rationales of gold nanoparticles for cancer theranostics, Adv Mater 28 (39) (2016) 8567–8585.
[8] W. Wu, et al., Designed synthesis and surface engineering strategies of magnetic iron oxide nanoparticles for biomedical applications, Nanoscale 8 (47) (2016) 19421–19474.
[9] K.D. Patel, et al., Carbon-based nanomaterials as an emerging platform for theranostics, Mater. Horiz. 6 (36) (2019) 434–469.
[10] C. Qi, et al., Calcium-based biomaterials for diagnosis, treatment, and theranostics, Chem. Soc. Rev. 47 (2) (2018) 357–403.
[11] C. Caltagirone, et al., Silica-based nanoparticles: a versatile tool for the development of efficient imaging agents, Chem. Soc. Rev. 44 (14) (2015) 4645–4671.
[12] W.Q. Lim, et al., Recent advances in multifunctional silica-based hybrid nanocarriers for bioimaging and cancer therapy, Nanoscale 8 (25) (2016) 12510–12519.
[13] R.K. Singh, et al., Progress in nanotheranostics based on mesoporous silica nanomaterial platforms, ACS Appl. Mater. Interfaces 9 (12) (2017) 10309–10337.
[14] B. Guo, et al., Molecular engineering of conjugated polymers for biocompatible organic nanoparticles with highly efficient photoacoustic and photothermal performance in cancer theranostics, ACS Nano 11 (10) (2017) 10124–10134.
[15] M. Araujo, et al., Natural melanin: a potential pH-responsive drug release device, Int J Pharm 469 (1) (2014) 140–145.
[16] M. Chu, et al., Melanin nanoparticles derived from a homology of medicine and food for sentinel lymph node mapping and photothermal in vivo cancer therapy, Biomaterials 91 (2016) 182–199.
[17] M. d'Ischia, et al., Melanins and melanogenesis: from pigment cells to human health and technological applications, Pigment Cell Melanoma Res 28 (5) (2015) 520–544.
[18] L. Tian, et al., Melanin-like nanoparticles: advances in surface modification and tumour photothermal therapy, J Nanobiotechnology 20 (1) (2022) 485.
[19] I. Marcovici, et al., Melanin and melanin-functionalized nanoparticles as promising tools in cancer research-A review, Cancers 14 (7) (2022) 1838.
[20] Y. Yue, X. Zhao, Melanin-like nanomedicine in photothermal therapy applications, Int. J. Mol. Sci. 22 (1) (2021) 399.
[21] H. Liu, et al., Melanin-like nanomaterials for advanced biomedical applications: a versatile platform with extraordinary promise, Adv. Sci. 7 (7) (2020), 1903129.
[22] L. Hong, J.D. Simon, Current understanding of the binding sites, capacity, affinity, and biological significance of metals in melanin, J. Phys. Chem. B 111 (28) (2007) 7938–7947.
[23] D.J. Kim, et al., The synthetic melanin nanoparticles having an excellent binding capacity of heavy metal ions, Bull. Kor. Chem. Soc. 33 (11) (2012) 3788–3792.
[24] A. Chen, et al., The effect of metal ions on endogenous melanin nanoparticles used as magnetic resonance imaging contrast agents, Biomater. Sci. 8 (1) (2020) 379–390.
[25] A. Liopo, et al., Melanin nanoparticles as a novel contrast agent for optoacoustic tomography, Photoacoustics 3 (1) (2015) 35–43.
[26] M. Kim, et al., Thermohydrogel containing melanin for photothermal cancer therapy, Macromol. Biosci. 17 (5) (2017).
[27] B. Poinard, et al., Polydopamine nanoparticles enhance drug release for combined photodynamic and photothermal therapy, ACS Appl. Mater. Interfaces 10 (25) (2018) 21125–21136.
[28] R. Zhang, et al., Engineering melanin nanoparticles as an efficient drug-delivery system for imaging-guided chemotherapy, Adv Mater 27 (34) (2015) 5063–5069.
[29] Z. Wang, et al., Application of polydopamine in tumor targeted drug delivery system and its drug release behavior, J Control Release 290 (2018) 56–74.
[30] Y. Liu, et al., Comprehensive insights into the multi-antioxidative mechanisms of melanin nanoparticles and their application to protect brain from injury in ischemic stroke, J. Am. Chem. Soc. 139 (2) (2017) 856–862.
[31] K.Y. Ju, et al., Bioinspired polymerization of dopamine to generate melanin-like nanoparticles having an excellent free-radical-scavenging property, Biomacromolecules 12 (3) (2011) 625–632.
[32] J. Hu, et al., Polydopamine free radical scavengers, Biomater. Sci. 8 (18) (2020) 4940–4950.
[33] L. Panzella, et al., Atypical structural and pi-electron features of a melanin polymer that lead to superior free-radical-scavenging properties, Angew Chem. Int. Ed. Engl. 52 (48) (2013) 12684–12687.
[34] Z. Yang, et al., A bioinspired strategy toward UV absorption enhancement of melanin-like polymers for Sun protection, CCS Chem. 5 (10) (2023) 2389–2402.
[35] Q. Fan, et al., Transferring biomarker into molecular probe: melanin nanoparticle as a naturally active platform for multimodality imaging, J. Am. Chem. Soc. 136 (43) (2014) 15185–15194.
[36] L. Zhang, et al., A multifunctional platform for tumor angiogenesis-targeted chemo-thermal therapy using polydopamine-coated gold nanorods, ACS Nano 10 (11) (2016) 10404–10417.
[37] T. Iwasaki, et al., Melanin precursor influence on structural colors from artificial melanin particles: PolyDOPA, polydopamine, and polynorepinephrine, Langmuir 34 (39) (2018) 11814–11821.
[38] W. Cao, et al., Radical-enriched artificial melanin, Chem. Mater. 32 (13) (2020) 5759–5767.
[39] U.J. Lee, et al., Light-triggered in situ biosynthesis of artificial melanin for skin protection, Adv. Sci. 9 (7) (2022), e2103503.
[40] C. Qi, et al., Melanin/polydopamine-based nanomaterials for biomedical applications, Sci. China Chem. 62 (2) (2019) 162–188.
[41] M. Caldas, et al., Melanin nanoparticles as a promising tool for biomedical applications - a review, Acta Biomater. 105 (2020) 26–43.
[42] J. Park, et al., Recent advances in melanin-like nanomaterials in biomedical applications: a mini review, Biomater. Res. 23 (1) (2019) 24.
[43] Y. Xiong, et al., Polydopamine-based nanocarriers for photosensitizer delivery, Front. Chem. 7 (2019) 471.
[44] Z. Wang, et al., Metal-containing polydopamine nanomaterials: catalysis, energy, and theranostics, Small 16 (18) (2020), e1907042.
[45] W. Cheng, et al., Versatile polydopamine platforms: synthesis and promising applications for surface modification and advanced nanomedicine, ACS Nano 13 (8) (2019) 8537–8565.
[46] I.S. Kwon, C.J. Bettinger, Polydopamine nanostructures as biomaterials for medical applications, J. Mater. Chem. B 6 (43) (2018) 6895–6903.
[47] P. Yang, et al., Stimuli-responsive polydopamine-based smart materials, Chem. Soc. Rev. 50 (14) (2021) 8319–8343.
[48] S. Singla, et al., Isolation and characterization of allomelanin from pathogenic black knot fungus-a sustainable source of melanin, ACS Omega 6 (51) (2021) 35514–35522.
[49] L.M. Martinez, et al., Production of melanins with recombinant microorganisms, Front. Bioeng. Biotechnol. 7 (2019) 285.
[50] M. d'Ischia, et al., Melanin biopolymers: tailoring chemical complexity for materials design, Angew Chem. Int. Ed. Engl. 59 (28) (2019) 11196–11205.
[51] W. Cao, et al., Unraveling the structure and function of melanin through synthesis, J. Am. Chem. Soc. 143 (7) (2021) 2622–2637.
[52] M. d'Ischia, et al., Polydopamine and eumelanin: from structure–property relationships to a unified tailoring strategy, Acc. Chem. Res. 47 (12) (2014) 3541–3550.
[53] N.E. El-Naggar, W.I.A. Saber, Natural melanin: current trends, and future approaches, with especial reference to microbial source, Polymers 14 (7) (2022) 1339.
[54] W. Yu, et al., Rescuing ischemic stroke by biomimetic nanovesicles through accelerated thrombolysis and sequential ischemia-reperfusion protection, Acta Biomater. 140 (2022) 625–640.
[55] S. Sheng, et al., Endogenous biocatalytic reaction-based nanoplatform for multifunctional tumor theranostics, Chem. Mater. 34 (19) (2022) 8664–8674.
[56] Y.S. Kwon, et al., Melanin-like nanoparticles as an alternative to natural melanin in retinal pigment epithelium cells and their therapeutic effects against age-related macular degeneration, ACS Nano 16 (11) (2022) 19412–19422.
[57] R. Hou, et al., Therapeutic effect of natural melanin from edible fungus Auricularia auricula on alcohol-induced liver damage in vitro and in vivo, Food Sci. Hum. Wellness 10 (4) (2021) 514–522.

[58] A. Mejía-Caballero, et al., Biosynthesis of catechol melanin from glycerol employing metabolically engineered Escherichia coli, Microb. Cell Factories 15 (1) (2016) 161.
[59] S.-Y. Ahn, et al., Microbial production of melanin pigments from caffeic acid and L-tyrosine using Streptomyces glaucescens and FCS-ECH-Expressing Escherichia coli, Int. J. Mol. Sci. 22 (5) (2021) 2413.
[60] D.W. Zheng, et al., Hierarchical micro-/nanostructures from human hair for biomedical applications, Adv Mater 30 (27) (2018), e1800836.
[61] M. Xiao, et al., Elucidation of the hierarchical structure of natural eumelanins, J R Soc Interface 15 (140) (2018), 20180045.
[62] S. Hong, et al., Enzyme mimicking based on the natural melanin particles from human hair, iScience 23 (1) (2020), 100778.
[63] Q. Lei, et al., Microneedle patches integrated with biomineralized melanin nanoparticles for simultaneous skin tumor photothermal therapy and wound healing, Adv FuncMater 32 (22) (2022), 2113269.
[64] Y. Wang, et al., Superior performance of polyurethane based on natural melanin nanoparticles, Biomacromolecules 17 (11) (2016) 3782–3789.
[65] X. Guo, et al., Preparation of water-soluble melanin from squid ink using ultrasound-assisted degradation and its anti-oxidant activity, J. Food Sci. Technol. 51 (12) (2014) 3680–3690.
[66] R.H. Deng, et al., Nanoparticles from cuttlefish ink inhibit tumor growth by synergizing immunotherapy and photothermal therapy, ACS Nano 13 (8) (2019) 8618–8629.
[67] L. Rong, et al., Iron chelated melanin-like nanoparticles for tumor-associated macrophage repolarization and cancer therapy, Biomaterials 225 (2019), 119515.
[68] Y. Liang, et al., Functionalized natural melanin nanoparticle mimics natural peroxidase for total antioxidant capacity determination, Sensor. Actuator. B Chem. 359 (2022), 131541.
[69] J. Xie, et al., Ink melanin from Sepiapharaonis ameliorates colitis in mice via reducing oxidative stress, andprotecting the intestinal mucosal barrier, Food Res. Int. 151 (2022), 110888.
[70] J. Zhou, et al., Natural melanin/alginate hydrogels achieve cardiac repair through ROS scavenging and macrophage polarization, Adv. Sci. (2021), e2100505.
[71] Y. Zhang, et al., Mitochondrial targeted melanin@mSiO2 yolk-shell nanostructures for NIR-II-driven photo-thermal-dynamic/immunotherapy, Chem. Eng. J. 435 (2022), 134869.
[72] P.K. Binsi, et al., Photo-protective effect of cuttlefish ink melanin on human hair, J. Appl. Polym. Sci. 139 (7) (2021), 51631.
[73] Z.Y. Hong, et al., Melanin-based nanomaterials: the promising nanoplatforms for cancer diagnosis and therapy, Nanomedicine 28 (2020), 102211.
[74] Y. Liu, et al., Polydopamine and its derivative materials: synthesis and promising applications in energy, environmental, and biomedical fields, Chem Rev 114 (9) (2014) 5057–5115.
[75] Q. Lyu, et al., Unravelling the polydopamine mystery: is the end in sight? Polym. Chem. 10 (42) (2019) 5771–5777.
[76] M. d'Ischia, et al., Melanin biopolymers: tailoring chemical complexity for materials design, Angew Chem. Int. Ed. Engl. 59 (28) (2020) 11196–11205.
[77] X. Wang, et al., Size control synthesis of melanin-like polydopamine nanoparticles by tuning radicals, Polym. Chem. 10 (30) (2019) 4194–4200.
[78] Z.E. Siwicka, et al., Synthetic porous melanin, J. Am. Chem. Soc. 143 (8) (2021) 3094–3103.
[79] D. Wu, et al., Mesoporous polydopamine carrying manganese carbonyl responds to tumor microenvironment for multimodal imaging-guided cancer therapy, Adv. Funct. Mater. 29 (16) (2019), 1900095.
[80] S. Wang, et al., Superfast and controllable microfluidic inking of anti-inflammatory melanin-like nanoparticles inspired by cephalopods, Mater. Horiz. 7 (2020) 1573–1580.
[81] P. Yang, et al., Structural and functional tailoring of melanin-like polydopamine radical scavengers, CCS Chem. 2 (2) (2020) 128–138.
[82] P. Yang, et al., Manipulating the antioxidative capacity of melanin-like nanoparticles by involving condensation polymerization, Sci. China Chem. 66 (5) (2023) 1520–1528.
[83] Y. Zou, et al., Regulating the absorption spectrum of polydopamine.pdf, Sci. Adv. 6 (36) (2020), eabb4696.
[84] P. Yang, et al., Tailoring synthetic melanin nanoparticles for enhanced photothermal therapy, ACS Appl. Mater. Interfaces 11 (45) (2019) 42671–42679.
[85] Y. Zou, et al., Photothermal-enhanced synthetic melanin inks for near-infrared imaging, Polymer 186 (2020), 122042.
[86] H. Zhang, et al., Synthetic fungal melanin nanoparticles with excellent antioxidative property, Giant 12 (2022), 100120.
[87] X. Zhou, et al., Artificial allomelanin nanoparticles, ACS Nano 13 (10) (2019) 10980–10990.
[88] F. Solano, Melanin and melanin-related polymers as materials with biomedical and biotechnological applications-cuttlefish ink and mussel foot proteins as inspired biomolecules, Int. J. Mol. Sci. 18 (7) (2017) 1561.
[89] C. Cavallini, et al., Melanin and melanin-like hybrid materials in regenerative medicine, Nanomaterials 10 (8) (2020) 1518.
[90] A. Capucciati, et al., Water-soluble melanin-protein-Fe/Cu conjugates derived from norepinephrine as reliable models for neuromelanin of human brain locus coeruleus, Angew Chem. Int. Ed. Engl. 61 (32) (2022), e202204787.
[91] E. Terreno, et al., Image guided therapy: the advent of theranostic agents, J Control Release 161 (2) (2012) 328–337.
[92] B.R. Smith, S.S. Gambhir, Nanomaterials for in vivo imaging, Chem Rev 117 (3) (2017) 901–986.
[93] J.-J. Liu, et al., RGD-functionalised melanin nanoparticles for intraoperative photoacoustic imaging-guided breast cancer surgery, Eur. J. Nucl. Med. Mol. Imag. 49 (3) (2021) 847–860.
[94] X. Yi, et al., Biomimetic copper sulfide for chemo-radiotherapy: enhanced uptake and reduced efflux of nanoparticles for tumor cells under ionizing radiation, Adv Func Mater 28 (9) (2018), 1705161.
[95] D.L. Longo, et al., Water soluble melanin derivatives for dynamic contrast enhanced photoacoustic imaging of tumor vasculature and response to antiangiogenic therapy, Adv Healthc Mater 6 (1) (2017), 1600550.
[96] Q. Jiang, et al., Red blood cell membrane-camouflaged melanin nanoparticles for enhanced photothermal therapy, Biomaterials 143 (2017) 29–45.
[97] Q. Jiang, et al., Erythrocyte-cancer hybrid membrane-camouflaged melanin nanoparticles for enhancing photothermal therapy efficacy in tumors, Biomaterials 192 (2019) 292–308.
[98] C. Qi, et al., Melanin-instructed biomimetic synthesis of copper sulfide for cancer phototheranostics, Chem. Eng. J. 388 (2020), 124232.
[99] Y. Li, et al., Targeted polydopamine nanoparticles enable photoacoustic imaging guided chemo-photothermal synergistic therapy of tumor, Acta Biomater. 47 (2017) 124–134.
[100] H. Shi, et al., Copper(II)-disulfiram loaded melanin-dots for cancer theranostics, Nanomedicine 32 (2021), 102340.
[101] C. Li, et al., Photoacoustic imaging-guided chemo-photothermal combinational therapy based on emissive Pt(II) metallacycle-loaded biomimic melanin dots, Sci. China Chem. 64 (1) (2020) 134–142.
[102] B. Fan, et al., Photoacoustic-imaging-guided therapy of functionalized melanin nanoparticles: combination of photothermal ablation and gene therapy against laryngeal squamous cell carcinoma, Nanoscale 11 (13) (2019) 6285–6296.
[103] J. Zhang, et al., From biology to biology: hematoporphyrin-melanin nanoconjugates with synergistic sonodynamic-photothermal effects on malignant tumors, Chem. Eng. J. 408 (2021), 127282.
[104] Y. Li, et al., Photothermal therapy-induced immunogenic cell death based on natural melanin nanoparticles against breast cancer, Chem. Commun. 56 (9) (2020) 1389–1392.
[105] S. Xiao, et al., Tracking osteoarthritis progress through cationic nanoprobe-enhanced photoacoustic imaging of cartilage, Acta Biomater. 109 (2020) 153–162.
[106] C. Zhao, et al., Structural transformative antioxidants for dual-responsive anti-inflammatory delivery and photoacoustic inflammation imaging, Angew Chem. Int. Ed. Engl. 60 (26) (2021) 14458–14466.
[107] C. Zhao, et al., Site-specific biomimicry of antioxidative melanin formation and its application for acute liver injury therapy and imaging, Adv Mater (2021), e2102391.
[108] X. Zhao, et al., An auto-photoacoustic melanin-based drug delivery nano-platform for self-monitoring of acute kidney injury therapy via a triple-collaborative strategy, Acta Biomater. 147 (2022) 327–341.
[109] H. Zhao, et al., Polydopamine nanoparticles for the treatment of acute inflammation-induced injury, Nanoscale 10 (15) (2018) 6981–6991.
[110] Z.-H. Miao, et al., Intrinsically Mn2+-chelated polydopamine nanoparticles for simultaneous magnetic resonance imaging and photothermal ablation of cancer cells, ACS Appl. Mater. Interfaces 7 (31) (2015) 16946–16952.
[111] Z. Dong, et al., Polydopamine nanoparticles as a versatile molecular loading platform to enable imaging-guided cancer combination therapy, Theranostics 6 (7) (2016) 1031–1042.
[112] Y. Wang, et al., Multifunctional melanin-like nanoparticles for bone-targeted chemo-photothermal therapy of malignant bone tumors and osteolysis, Biomaterials 183 (2018) 10–19.
[113] S. Kang, et al., T1-Positive Mn(2+)-doped multi-stimuli responsive poly(L-DOPA) nanoparticles for photothermal and photodynamic combination cancer therapy, Biomedicines 8 (10) (2020) 417.
[114] N. Xu, et al., Fe(III)-Chelated polydopamine nanoparticles for synergistic tumor therapies of enhanced photothermal ablation and antitumor immune activation, ACS Appl. Mater. Interfaces 14 (14) (2022) 15894–15910.
[115] H. Zhou, et al., (64)Cu-labeled melanin nanoparticles for PET/CT and radionuclide therapy of tumor, Nanomedicine 29 (2020), 102248.
[116] J. Yan, et al., Melanin nanoparticles as an endogenous agent for efficient iron overload therapy, J. Mater. Chem. B 4 (45) (2016) 7233–7240.
[117] J. Sheng, et al., Theranostic radioiodine-labelled melanin nanoparticles inspired by clinical brachytherapy seeds, J. Mater. Chem. B 6 (48) (2018) 8163–8169.
[118] Y. Yue, et al., Biomimetic nanoparticles carrying a repolarization agent of tumor-associated macrophages for remodeling of the inflammatory microenvironment following photothermal therapy, ACS Nano 15 (9) (2021) 15166–15179.
[119] C. Xue, et al., NIR-actuated remote activation of ferroptosis in target tumor cells through a photothermally responsive iron-chelated biopolymer nanoplatform, Angew Chem. Int. Ed. Engl. 60 (16) (2021) 8938–8947.
[120] G. Yang, et al., Polydopamine-engineered theranostic nanoscouts enabling intracellular HSP90 mRNAs fluorescence detection for imaging-guided chemo-photothermal therapy, Adv Healthc Mater (2022), e2201615.
[121] Q. Zou, et al., Functional nanomaterials based on self-assembly of endogenic NIR-absorbing pigments for diagnostic and therapeutic applications, Small Methods 6 (4) (2022), e2101359.
[122] Y. Liu, et al., Photoacoustic molecular imaging: from multiscale biomedical applications towards early-stage theranostics, Trends Biotechnol. 34 (5) (2016) 420–433.
[123] B. Zhu, et al., Photoacoustic microscopic imaging of cerebral vessels for intensive monitoring of metabolic acidosis, Mol. Imag. Biol. 25 (4) (2023) 659–670.

[124] J. Zhang, et al., In vivo characterization and analysis of glioblastoma at different stages using multiscale photoacoustic molecular imaging, photoacoustics 30 (2022), 100462.
[125] Y. Liu, et al., Photothermal therapy and photoacoustic imaging via nanotheranostics in fighting cancer, Chem. Soc. Rev. 48 (7) (2019) 2053–2108.
[126] W. Fan, et al., Nanotechnology for multimodal synergistic cancer therapy, Chem Rev 117 (22) (2017) 13566–13638.
[127] C.Y. Lin, et al., Photoacoustic imaging for noninvasive periodontal probing depth measurements, J. Dent. Res. 97 (1) (2018) 23–30.
[128] K.-Y. Ju, et al., pH-Induced aggregated melanin nanoparticles for photoacoustic signal amplification, Nanoscale 8 (30) (2016) 14448–14456.
[129] W. Yim, et al., Enhanced photoacoustic detection of heparin in whole blood via melanin nanocapsules carrying molecular agents, ACS Nano 16 (2021) 683–693.
[130] T. Repenko, et al., Strong photoacoustic signal enhancement by coating gold nanoparticles with melanin for biomedical imaging, Adv. Funct. Mater. 28 (7) (2018), 1705607.
[131] B. Silvestri, et al., Silver-nanoparticles as plasmon-resonant enhancers for eumelanin's photoacoustic signal in a self-structured hybrid nanoprobe, Mater. Sci. Eng. C 102 (2019) 788–797.
[132] K.Y. Ju, et al., Bio-inspired, melanin-like nanoparticles as a highly efficient contrast agent for T1-weighted magnetic resonance imaging, Biomacromolecules 14 (10) (2013) 3491–3497.
[133] S.J. Liu, et al., A promising magnetic resonance stem cell tracer based on natural biomaterials in a biological system: manganese(II) chelated to melanin nanoparticles, Int. J. Nanomed. 13 (2018) 1749–1759.
[134] W.W. Cai, et al., Effective tracking of bone mesenchymal stem cells in vivo by magnetic resonance imaging using melanin-based gadolinium(3+) nanoparticles, J. Biomed. Mater. Res. 105 (1) (2017) 131–137.
[135] W. Xu, et al., Melanin-manganese nanoparticles with ultrahigh efficient clearance in vivo for tumor-targeting T1 magnetic resonance imaging contrast agent, Biomater. Sci. 6 (1) (2017) 207–215.
[136] L. Xu, et al., Dual T1 and T2 weighted magnetic resonance imaging based on Gd(3+) loaded bioinspired melanin dots, Nanomedicine 14 (6) (2018) 1743–1752.
[137] Y. Li, et al., Structure and function of iron-loaded synthetic melanin, ACS Nano 10 (11) (2016) 10186–10194.
[138] H. Liu, et al., Novel intrapolymerization doped manganese-eumelanin coordination nanocomposites with ultrahigh relaxivity and their application in tumor theranostics, Adv. Sci. 5 (7) (2018), 1800032.
[139] J.E. Lemaster, et al., Gadolinium doping enhances the photoacoustic signal of synthetic melanin nanoparticles: a dual modality contrast agent for stem cell imaging, Chem. Mater. 31 (1) (2018) 251–259.
[140] Z. Wang, et al., High relaxivity gadolinium-polydopamine nanoparticles, Small 13 (43) (2017), 1701830.
[141] R. Chakravarty, et al., Positron emission tomography image-guided drug delivery: current status and future perspectives, Mol. Pharm. 11 (11) (2014) 3777–3797.
[142] Q. Liu, et al., pH-triggered assembly of natural melanin nanoparticles for enhanced PET imaging, Front. Chem. 8 (2020) 755.
[143] P. Zhang, et al., Pharmacokinetics study of Zr-89-labeled melanin nanoparticle in iron-overload mice, Nucl. Med. Biol. 43 (9) (2016) 529–533.
[144] X. Bao, et al., Polydopamine nanoparticles as efficient scavengers for reactive oxygen species in periodontal disease, ACS Nano 12 (9) (2018) 8882–8892.
[145] C. Li, et al., Near-infrared metal agents assisting precision medicine: from strategic design to bioimaging and therapeutic applications, Chem. Soc. Rev. 52 (13) (2023) 4392–4442.
[146] Y. Xu, et al., Long wavelength–emissive Ru(II) metallacycle–based photosensitizer assisting in vivo bacterial diagnosis and antibacterial treatment, Proc. Natl. Acad. Sci. USA 119 (32) (2022), e2209904119.
[147] Y. Xu, et al., Construction of a 980 nm laser-activated Pt(II) metallacycle nanosystem for efficient and safe photo-induced bacteria sterilization, Sci. China Chem. 66 (1) (2022) 155–163.
[148] J. Dong, et al., A natural cuttlefish melanin nanoprobe for preoperative and intraoperative mapping of lymph nodes, Nanomedicine 41 (2021), 102510.
[149] J. Sun, et al., Ultrasmall endogenous biopolymer nanoparticles for magnetic resonance/photoacoustic dual-modal imaging-guided photothermal therapy, Nanoscale 10 (22) (2018) 10584–10595.
[150] L. Zhang, et al., Bioinspired multifunctional melanin-based nanoliposome for photoacoustic/magnetic resonance imaging-guided efficient photothermal ablation of cancer, Theranostics 8 (6) (2018) 1591–1606.
[151] Z. Zhou, et al., Melanin-like nanoparticles decorated with an autophagy-inducing peptide for efficient targeted photothermal therapy, Biomaterials 203 (2019) 63–72.
[152] T. Feng, et al., Dual-stimuli responsive nanotheranostics for mild hyperthermia enhanced inhibition of Wnt/β-catenin signaling, Biomaterials 232 (2020), 119709.
[153] K. Chen, et al., Biocompatible melanin based theranostic agent for in vivo detection and ablation of orthotopic micro-hepatocellular carcinoma, Biomater. Sci. 8 (15) (2020) 4322–4333.
[154] D. Sun, et al., Intrinsically bioactive manganese-eumelanin nanocomposites mediated antioxidation and anti-neuroinflammation for targeted theranostics of traumatic brain injury, Adv Healthc Mater 11 (16) (2022), e2200517.
[155] W. Cai, et al., NIR-II FL/PA dual-modal imaging long-term tracking of human umbilical cord-derived mesenchymal stem cells labeled with melanin nanoparticles and visible HUMSC-based liver regeneration for acute liver failure, Biomater. Sci. 8 (23) (2020) 6592–6602.
[156] Y. Sun, et al., Melanin-dot-mediated delivery of metallacycle for NIR-II/photoacoustic dual-modal imaging-guided chemo-photothermal synergistic therapy, Proc Natl Acad Sci U S A 116 (34) (2019) 16729–16735.
[157] S. Cho, et al., Silica-coated metal chelating-melanin nanoparticles as a dual-modal contrast enhancement imaging and therapeutic agent, ACS Appl. Mater. Interfaces 9 (1) (2017) 101–111.
[158] T. Sun, et al., A melanin-based natural antioxidant defense nanosystem for theranostic application in acute kidney injury, Adv. Funct. Mater. 29 (48) (2019), 1904833.
[159] Q. Zhang, et al., Hierarchically nanostructured hybrid platform for tumor delineation and image-guided surgery via NIR-II fluorescence and PET bimodal imaging, Small 15 (45) (2019), e1903382.
[160] J. Sun, et al., A dual-modality MR/PA imaging contrast agent based on ultrasmall biopolymer nanoparticles for orthotopic hepatocellular carcinoma imaging, Int. J. Nanomed. 14 (2019) 9893–9904.
[161] J. Sun, et al., Facile synthesis of melanin-dye nanoagent for NIR-II fluorescence/photoacoustic imaging-guided photothermal therapy, Int. J. Nanomed. 15 (2020) 10199–10213.
[162] B. Qu, et al., IR820 functionalized melanin nanoplates for dual-modal imaging and photothermal tumor eradication, Nanoscale Adv. 2 (6) (2020) 2587–2594.
[163] S. He, et al., Crucial breakthrough of second near-infrared biological window fluorophores: design and synthesis toward multimodal imaging and theranostics, Chem. Soc. Rev. 47 (12) (2018) 4258–4278.
[164] Y. Deng, et al., Biomedical applications of fluorescent and magnetic resonance imaging dual-modality probes, Chembiochem 20 (4) (2019) 499–510.
[165] M. Yang, et al., Dragon fruit-like biocage as an iron trapping nanoplatform for high efficiency targeted cancer multimodality imaging, Biomaterials 69 (2015) 30–37.
[166] S.W. Ha, et al., Ions doped melanin nanoparticle as a multiple imaging agent, J Nanobiotechnology 15 (1) (2017) 73.
[167] S.H. Hong, et al., A chelator-free and biocompatible melanin nanoplatform with facile loading gadolinium and copper-64 for Bioimaging.pdf, Bioconjug Chem 28 (7) (2017) 1925–1930.
[168] J. Lin, et al., Multimodal-imaging-guided cancer phototherapy by versatile biomimetic theranostics with UV and gamma-irradiation protection, Adv Mater 28 (17) (2016) 3273–3279.
[169] S. Wang, et al., Core-satellite polydopamine-gadolinium-metallofullerene nanotheranostics for multimodal imaging guided combination cancer therapy, Adv Mater 29 (35) (2017), 1701013.
[170] J. Sun, et al., Multifunctional hybrid nanoprobe for photoacoustic/PET/MR imaging-guided photothermal therapy of laryngeal cancer, ACS Appl. Bio Mater. 4 (6) (2021) 5312–5323.
[171] Z. Wang, et al., In situ growth of Au nanoparticles on natural melanin as biocompatible and multifunctional nanoagent for efficient tumor theranostics, J. Mater. Chem. B 7 (1) (2019) 133–142.
[172] T. He, et al., Dual-stimuli-responsive nanotheranostics for dual-targeting photothermal-enhanced chemotherapy of tumor, ACS Appl. Mater. Interfaces 13 (19) (2021) 22204–22212.
[173] Z. Dong, et al., Synthesis of hollow biomineralized CaCO3-polydopamine nanoparticles for multimodal imaging-guided cancer photodynamic therapy with reduced skin photosensitivity, J. Am. Chem. Soc. 140 (6) (2018) 2165–2178.
[174] L. Xia, et al., A highly specific multiple enhancement theranostic nanoprobe for PET/MRI/PAI image-guided radioisotope combined photothermal therapy in prostate Cancer.pdf, Small 17 (21) (2021), 2100378.